Application of Deuterium Isotope Effects on NMR Parameters as a Method of Intramolecular Hydrogen Bond Characterization in Enolic Forms of 1,3-diketones in the Solid State

by

Maria Anna Matlinska

A thesis submitted in partial fulfillment of the requirements for the degree of

Master of Science

Department of Chemistry
University of Alberta

Abstract

The application of deuterium isotope effects on ^{13}C NMR chemical shifts to study the nature of intramolecular hydrogen bonding in the enolic forms of two 1,3-diketones, tetraacetylethane (TAE) and avobenzone, in the solid state is reported. Carbon-13 NMR spectra of natural abundance TAE and deuterium-labelled TAE (TAE-OD) obtained at room temperature show a deuterium shift of 1.0 ppm on one of the two enolic carbon nuclei. The deuterium isotope effect of 2.4 ppm at 163 K is reported. The position of the enolic hydrogen is determined as favoring one side on the molecule, confirming the asymmetric nature of the hydrogen bond. This finding is consistent with variable temperature neutron diffraction data, which is one of the most reliable methods of hydrogen position determination.

In case of avobenzone, the apparent deuterium isotope effect on the enolic carbon on the *tert*-butyl side of the molecule is 1.3 ppm at room temperature and 2.0 ppm at 185 K. This is the largest deuterium isotope effect on carbon chemical shifts reported so far in the literature for enolic forms of 1,3-diketones. Moreover, variable temperature ^{13}C spectra show temperature-dependent line shapes, indicating unusual intramolecular dynamics i.e., rapid flips of the methoxybenzene fragment of the molecule. This allowed to estimate the energy barrier of the methoxybenzene ring rotation that was found to be approximately 57 kJ mol^{-1}.

The experimental data supplemented by computational results indicates how a distinct behavior of the enol-bound carbon allows the determination of the position of the hydrogen in the keto-enol part of the molecule. The research presented in this thesis illustrates the application of deuterium isotope effects on ^{13}C NMR parameters in the characterization of hydrogen bonding in the solid state. This thesis offers a distinctive insight into measuring NMR deuterium isotope effects on carbon-13 nuclei in the solid state, filling a substantial gap in the current literature.

Dedication

To all past, present, and future Scientists representing the marginalized groups.

With hope that the time when we are all treated like truly equal comes very soon.

Acknowledgments

I would like to formally acknowledge and thank for the help provided to me by many people during my research. I thank my supervisor, Prof. Roderick E. Wasylishen for sharing his expertise, enthusiasm, patience, and kindness, as well as supporting me throughout the duration of my graduate program and the completion of this thesis. I thank Dr. Guy M. Bernard for providing me with training and assistance required for performing the solid-state NMR experiments and data analysis. I thank Mr. Mark Miskolzie and Ms. Nupur Dabral for their assistance and expertise in acquiring the solution NMR spectra. I thank Dr. James M. Hook for providing preliminary solution and variable temperature solid-state NMR spectra of avobenzone at B_o 7.05 T. I thank Dr. Victor V. Terskikh for performing NMR experiments and result analysis on natural abundance solid-state avobenzone and tetraacetylethane at 21.1 T magnetic field. I thank Dr. Andreas Brinkmann for performing CASTEP calculations on avobenzone and tetraacetylethane. I thank Dr. Michael Ferguson and Dr. Robert McDonald for their assistance with single crystal X-ray diffraction experiments and obtaining structures of the compounds included in my research.

I thank staff members of the Chemistry NMR Facility supervised by Dr. Ryan McKay and the staff of the Machine Shop for providing necessary equipment adjustments that improved accessibility and allowed me to perform experiments independently.

I would like to acknowledge the past work of Colleagues who contributed to this project in a broader context at various stages of its development, prior to my involvement.

I thank the members of my supervisory committee, Prof. Jillian Buriak and Prof. Wolfgang Jaeger for their time, expertise, and feedback throughout the duration of my

research and completion of the thesis. I thank Prof. Michael Serpe for serving on my examining committee. I thank the Alberta Innovates for awarding me a two-year funding.

Table of Contents

LIST OF TABLES

LIST OF FIGURES

LIST OF SYMBOLS

$^{n}\Delta C(D)$ = deuterium isotope effect on ^{13}C NMR chemical shift

n = number of bonds between the carbon in question and the deuterium atom

$\delta C(H)$ = chemical shift of carbon bonded to the hydrogen atom

$\delta C(D)$ = chemical shift of carbon bonded to the deuterium atom

$(\Delta\delta$ H,D) = change in chemical shifts upon deuteration

δ_{OHO} = ^{1}H NMR chemical shift of the enolic proton

Δ_{obs} = observed isotope shift

Δ_{o} = isotope effect due to the presence of a heavier nucleus

Δ_{eq} = perturbation of the equilibrium

τ^{c} = lifetime of a nucleus is equal at site A and X

$(\nu_A - \nu_X)$ = chemical shift difference between site A and site X, in Hz in the absence of exchange

κ = transmission coefficient

k_B = Boltzmann constant

h = Planck constant,

R = molar gas constant

T = absolute temperature at coalescence

$\Delta G\dagger$ = free energy of activation of the methoxyphenyl ring flip

1. Introduction

1.1. Background

1.1.1. Thesis Goal

The goal of this research is to present the application of deuterium isotope effects on ^{13}C NMR chemical shifts as an important method of characterizing intramolecular hydrogen-bonds in solids. Using enolic forms of selected 1,3-β-diketones, and their deuterium-labelled analogues, the research illustrates the value of isotope effect measurements in studying a class of intramolecularly hydrogen-bonded systems, which have been comprehensively studied via solution NMR. The additional insight provided by solid-state NMR includes identifying the enolic hydrogen position and in some cases allowing probing molecular dynamics in the solid state. Those features often cannot be determined by solution NMR due to the rapid molecular tumbling. Examples presented in this work demonstrate the advantage of solid-state NMR techniques over solution NMR in studying an important class of intramolecularly hydrogen-bonded systems, especially if the two enol forms are related by symmetry.

1.1.2. Hydrogen Bonding

There is no ideal definition of hydrogen bonding, and various criteria have been proposed over the years. The purpose of this section is to provide brief and general understanding of this interaction, while acknowledging that hydrogen bond complexity and diversity cannot be reduced to a one-sentence statements thus a comprehensive literature review is recommended.[10–13] Hydrogen bonding is a donor-acceptor interaction, formed when an atom A is of greater electronegativity relative to H atom, such as to withdraw electron density and leave the proton partially deshielded.[14] T. Steiner proposed a definition in terms of donating proton, and not electron withdrawal. An X-H…A interaction is a hydrogen bond, if it constitutes a local bond and X-H acts as proton donor to A.[13]

1. Introduction

1.1. Background

The definition proposed by IUPAC states that in a bond depicted as X-H…Y-Z (dots denote the bond) it is an attractive interaction between a hydrogen from a molecule or molecular fragment X-H, where X is more electronegative than H and an atom or a group of atoms in the same or a different molecule, in which there is evidence of bond formation.[10]

Intramolecular hydrogen bonds are particularly interesting, as they affect electronic distribution, molecular geometry, impacting greatly molecular properties and interactions. My work focuses on intramolecular hydrogen bonding in the O-H-O fragments of 1,3-β-diketones in their enolic forms.

Historically, the unusual properties of water played an important role in introducing the concept of the hydrogen bond. Despite having a small molecular weight, water has an incredibly high boiling point of 100 ^{o}C, and high freezing point of 0 ^{o}C. When boiling points of liquids typically increase with molecular weight (b.p. of F_2 is -188 ^{o}C while that of Cl_2 is -34 ^{o}C), and the boiling point of hydrogen sulfide is -62 ^{o}C, it was difficult to rational the unusual behavior of water without introducing the idea of a strong intermolecular interaction.[14–17]

Hydrogen bonding plays an important role both in biology, for example in stabilizing the DNA structure as well as in functional materials, such as chemosensors and pharmaceuticals.[18,19] Some examples include the role of hydrogen bonding in the formation of co-crystals, such as those of anti-tuberculosis drug pyrazinamide or a common painkiller acetaminophen.[20] The ability of hydrogen bond formation of these compounds allows a wide range of modifications to improve bioavailability and tune interactions with other active pharmaceutical ingredients.[20] It is also crucial in materials such as noxious gas sensors or enabling high-sensitivity self-healing materials used in human-machine interactions.[18,21]

1. Introduction

1.1. Background

1.1.3. 1,3-β-Diketones and their Enolic Forms

1,3-diketones are among the most significant classes of organic compounds due to their accessibility, stability, and often unique properties.[22] Their important applications include synthesis of core heterocycles crucial in medicinal chemistry (e.g. pyrazole, triazole), but also chelating ligand role for various metals in materials chemistry.[23] Substitution of a central carbon atom by nitrogen allows the formation of coordination complexes with a variety of uses, such as spin crossover materials, metal-organic frameworks (MOFs) and luminescent complexes.[24–26]

1,3-diketones consist of two keto groups separated by a methylene group, such as in acetylacetone (Figure 1).[16] They also provide the best-known examples of keto-enol tautomerism – the existence of more than one form of compound readily interconverting, in this case exchanging a hydrogen atom.[27] The relative amounts of the enol and keto tautomers are dictated by the properties of the solvent: the amount of the enol form increases with the decrease of solvents' dielectric constant.[28]

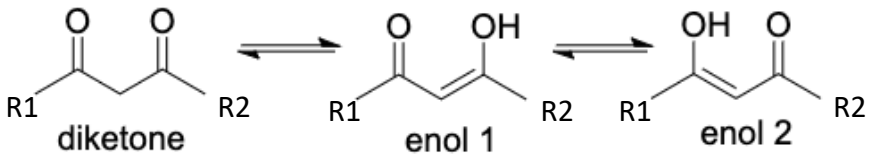

Figure 1. Acetylacetone molecule in its three tautomeric forms. In this case, R1 and R2 substituents are both methyl groups.

In non-symmetric compounds, where R1 and R2 are two different groups, the position of proton in the enolic tautomer is of interest from the perspective of fundamental science, as well as its practical implications. Transfer of proton from one oxygen atom to another in an intramolecular hydrogen bond belongs to one of the most important reactions in chemistry.[29] It plays a role in acid-base neutralization, and is crucial in biochemical processes, such as enzymatic reactions and tautomeric changes within DNA bases.[30]

1.1.4. Hydrogen Bonding Strength and Characterization Techniques

Hydrogen bond energies that exceed 50 kJ mol^{-1} are classified as strong and are characterized in several ways.[14] In the enol tautomer of 1,3-dicarbonyl compounds the O---O separation of 2.5 Å or less is generally classified as strong hydrogen bonding.[31] Moreover, they can be characterized by large infrared stretching frequency shifts and relatively large proton NMR chemical shifts.[14]

Characterization of hydrogen bonds in the solid state poses significant challenges. Neutron diffraction is considered the gold standard, as it can determine the position of hydrogen atoms with high accuracy, however high costs and low accessibility limit the use of this technique.[32]

X-ray diffraction is much less expensive and more accessible; however, it is much less accurate in determining the hydrogen atom positions and, similarly to neutron diffraction, is limited to crystalline materials.[33] Other techniques, such as electron diffraction or rotational spectroscopy are restricted to the gas phase, and relatively small molecules.[34,35]

Quantum chemistry computations are often used to model the character of hydrogen bonding. These include density-functional theory (DFT) methods, CASTEP (Cambridge Serial Total Energy Package) that can account for intermolecular interactions of molecules in the solid state.[36–40]

NMR spectroscopy is an important tool for structure elucidation applicable to gas, liquid, and solid phase materials. It offers several characterization probes, such as measurements of direct and indirect spin-spin couplings, variable temperature studies or measurements of deuterium isotope effects on ^{13}C chemical shifts.[3,41]

1. Introduction

1.2. Nuclear Magnetic Resonance in Hydrogen Bond Studies

1.2.1. Correlation between ^{1}H chemical shifts and O---O Separation Distance

One of the most basic and generally available NMR techniques used in studying the OHO systems depend on the correlation between ^{1}H chemical shifts of hydrogen-bonded atoms and the bond geometry, in particular the O---O separation distance.[3] Based on known neutron diffraction structures and ^{1}H chemical shifts measured in the solid state, scientists have proposed geometry correlations that are successfully used for the characterization of strong hydrogen bonds in biological systems.[42–45] Such correlations were also established for NHN- and NHO-systems and applied in the liquid state. [46–49]

To present an example of the experimentally obtained correlation of ^{1}H chemical shift with the deviation of the proton from the center of the resonance assisted hydrogen bond, the following symbols are introduced in Figure 2.

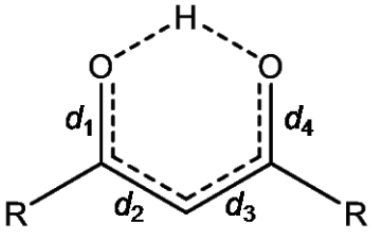

Figure 2. Resonance assisted hydrogen bonding structure for the keto-enol region of the β-diketone, with d_i defining bond lengths.[1,2]

The strength of the hydrogen bond may be assessed by the values of q_1 and q_2, defined in Equation 1 below.

Equation (1)

$$q_1 = d_4 - d_1$$
$$q_2 = d_2 - d_3$$

An example of the correlation of the experimentally obtained chemical shift with the deviation of q_1, which is position of the proton in relation to the center of the hydrogen bond has been published by Emmler et al. and is presented in Figure 3.[3]

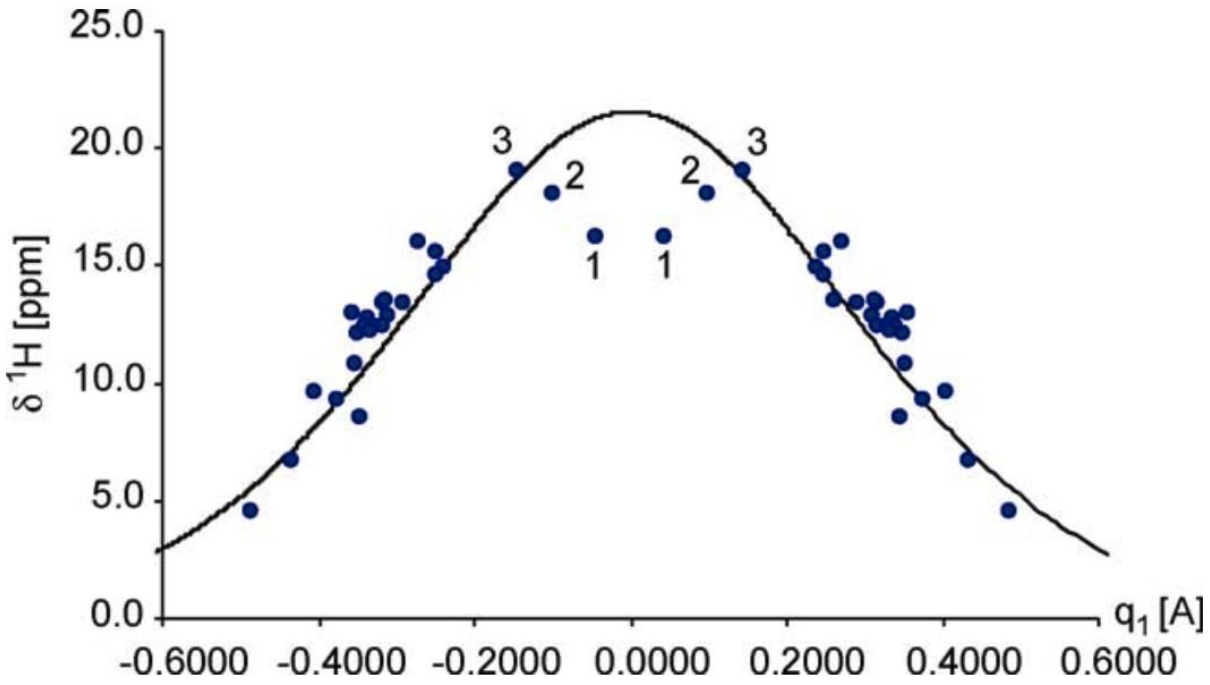

Figure 3. Correlation of the experimentally obtained chemical shift (blue dots) and the distance of the hydrogen atom from the center of the hydrogen bond *q1*. Black solid line represents the modelled correlation and the uncertainity of the measured chemical shift is approximately 0.1 ppm.[3]

In general, the closer the position of the hydrogen atom to the center of the hydrogen bond, the larger the ^{1}H chemical shift. The resulting curve resembles the transition of hydrogen atom from one side of the intramolecular hydrogen bond to the opposite site, through the middle position ($q_1 = 0$). The authors studied many different classes of compounds and the values for weak and intermediate hydrogen bonds are in excellent agreement with the correlation line. The scattering of data is explained by secondary structural effects. Significant deviations marked as

1 and 2 are due to the nature of energy potential well for the proton motion in these compounds (dibenzoylmethane and benzoylacetone) and its consequences are discussed in the publication.[3]

1.2.2. Deuterium Isotope Effects on ^{13}C Chemical Shifts

Upon substitution by a heavier atom, all resonant NMR nuclei in the molecule experience a slight chemical shift due to the change in rovibrational averaging of electronic properties of the molecules. The magnitude of the shift is related to the fractional change of mass upon substitution and is approximately proportional to the number of atoms substituted by the isotopes. The larger change in mass of the substituted isotope, the lower the zero-point energy of the vibration of the bond, and the greater the change in the shielding due to the isotope effect.[7,50–52]

Deuterium isotope effects are defined in Equation 2, where *n* is the number of bonds between the carbon in question and the deuterium.[50]

Equation (2)

$$^{n}\Delta C(D) = \delta C(H) - \delta C(D)$$

Benzene is a simple molecule that illustrates the one-, two- and three-bond deuterium isotope effects on ^{13}C shielding, chemical shifts (Figure 4).

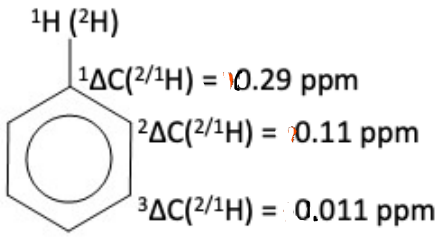

Figure 4. Benzene molecule with the values of one-, two- and three-bond deuterium isotope effects on ^{13}C NMR chemical shifts.[4]

1. Introduction

1.2. Nuclear Magnetic Resonance in Hydrogen Bond Studies

In general, the magnitude of isotope shifts depends on the distance of the isotopic substitution to from observed nucleus and is related to the chemical shift range of the observed nucleus. Moreover, the magnitudes of the isotope shifts are related to the fractional change in mass upon isotopic substitution.[53]

Deuteration of the hydroxyl group in an intramolecular hydrogen bonded system generally leads to greater shielding of the ^{13}C atoms bonded to that group.[54] Reuben has indicated that the magnitude of the isotope shift correlates with the energy of the hydrogen bond.[54] However, more specific nomenclature provided later refers to the hydrogen bond strength in terms of O---O separation and hydrogen bond geometry instead of the hydrogen bond energy and will be used in this thesis.[50–52,55,56]

Deuterium isotope effects on ^{13}C magnetic shielding have been extensively studied in a large variety of organic hydrogen-bonded compounds using solution NMR.[41,50–52,55] The two-bond isotope shift values usually do not exceed 1 ppm. Some tautomeric, unsymmetrical compounds with the O-H-O fragments have the isotope shifts as large as +1.91 ppm (2-acetylcyclohexanone), but these are rather uncommon.[50] In case of acetylacetone, +0.64 ppm is reported in $CDCl_3$.[50]

The extent of isotope effects in solution NMR studies shows the significance of this technique in the characterization of the hydrogen-bonded systems.[31,45,51,52,54–57] Unfortunately this area remains practically uncharted for compounds in the solid state. The motivation for my research is to propose a contribution that will fill a part of this gap. In the following chapters I will present solid-state ^{13}C NMR study of model enolic forms of compounds from the

1,3-diketones group at room and variable temperatures (VT), their deuterium isotope effects and the information about the character of their hydrogen bonding that can be extracted from the experimental data.

2. Compounds Studied

2.1. Tetraacetylethane

2.1.1. Background Information

Tetraacetylethane (TAE) is a dimer of acetylacetone (acac), occurring in the solid state in the form of white crystals with melting point in the 192-193 ^{o}C range.[58] It is commonly used in preparation of thermally stable polymers and as a bidental chelating ligand.[59] More recently, it has been used as a precursor to grow carbon nanowalls with flower-like morphology (CNW-LFs).[60]

TAE was chosen to study its intramolecular hydrogen bonding and the position of enolic hydrogen for several reasons. Firstly, it is a simple model compound, being the closest derivative of acetylacetone available naturally in the solid state at room temperature. It has been studied extensively, X-ray and more importantly, neutron diffraction data are available in the literature along with several computational studies.[5,58,61,62]

TAE has also been studied via solution and solid-state NMR.[63,64] Takegoshi and McDowell used single crystal solid-state NMR to determine the magnitudes and orientations of the ^{13}C chemical shielding tensors in TAE. They found that because the of the presence of a strong intramolecular hydrogen bond, the electronic environment around both carbonyl carbon nucleus and the enolic carbon nucleus are similar, suggesting conjugation within the keto-enol part.[63] Emsley et al.[64] used solution NMR to measure the ^{1}H chemical shifts of the enolic proton and change in chemical shifts upon deuteration ($\Delta\delta$ H,D) in TAE and three substituted TAE compounds to investigate the hydrogen bonding strength and factors affecting it. They found that the δ_{OHO} was independent of whether the substituted group was electron-withdrawing or electron-releasing, and ultimately steric effects were the reason of the changes in TAE O---O separation distances.[64]

2. Compounds Studied

2.1. Tetraacetylethane

Before discussing these results, it is worth to consider data collected for acetylacetone, a monomer in the structure of TAE. In solution, the keto-enol tautomerization of acac has been extensively studied, and the relative population of keto and enol forms depends on factors such as the dielectric constant of the solvent, temperature, and presence of other species capable of hydrogen bonding.[28,65,66] In the enolic form of acac in $CDCl_3$, the two carbon atoms bonded to oxygen are equivalent and their ^{13}C NMR chemical shift is 191.25 ppm, while the central carbon atom has a shift of 100.48 ppm.[67] Upon substitution of the enolic hydrogen with deuterium, the C-O carbon nuclei experience deuterium isotope shifts of 0.761 ppm at 220 K and 0.639 ppm at 300 K, however they remain equivalent in solution at any temperature due to the rapid exchange on the timescale of the experiment.[56]

The ^{13}C NMR spectrum of TAE in $CDCl_3$ solution does not distinguish carbon (CO) atoms, and the spectrum resembles that of acac. The two carbon atoms bonded to oxygen are slightly more deshielded with a shift of 192.71 ppm, while the central atom is approximately 8 ppm more deshielded comparing with acac (TAE shift of 108.16 ppm). For the full solution spectra of TAE, please see Appendix B.

Crystal Structures

In this section, X-ray diffraction studies of TAE are summarized to provide a historical context. However, the variable temperature neutron diffraction is the primary research used for work presented in this thesis.[6]

X-ray diffraction study conducted in 1966 showed that TAE belongs to orthorhombic space group *Pbcn* and exists in dienolic form.[58] It has crystallographic symmetry 2 (C_2) but approximates closely to $\bar{4}2m$ (D_{2d}) consisting of two substantially planar halves twisted through approximately 90° with respect to each other (Figure 5). The two C-O bonds have very similar

lengths (shorter C1-O1 of 1.295(6) Å and C3-O3 of 1.310(6) Å). The authors indicate that due to the absence of any short van der Waal's contacts, the hydrogen atom in each enolic group is involved in intramolecular hydrogen bonding, however the exact nature of that bonding could not be determined because the hydrogen atom position was not located. Regardless, it was concluded that the hydrogen bond was probably symmetric.

An early neutron diffraction study of TAE has confirmed the enolic nature of the compound, however the position of the enolic hydrogen was clearly asymmetric.[61] The space group was confirmed as orthorhombic *Pbcn,* and the dihedral angle between the two acetylacetone residues determined to be 92.4°. The C1-O1 and C3-O2 distances were 1.277(3) Å and 1.289(3) Å, respectively. Structural parameters obtained by neutron diffraction apart from hydrogen atom position, were consistent with the previous X-ray study.

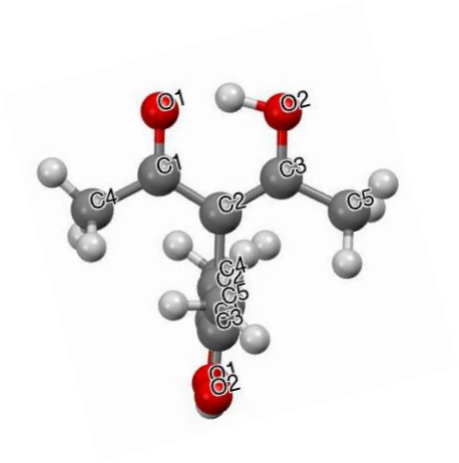

Figure 5. Molecule of TAE with two planar halves of the dimer perpendicular to each other. Crystal structure and atom numbering scheme presented after Lyssenko et al.[5]

Another structure analysis was performed as a response to the neutron diffraction study.[5,61] The neutron diffraction analysis at 298 K revealed a significant shortening of the O1-O2 distance in comparison to the acetylacetone monomer, as well as general equalization of all bond lengths within the keto-enol ring.[61] Lyssenko et al. obtained X-ray structure at 110 K, which

showed significant changes in comparison to the neutron diffraction data collected at 298 K.[29,6] It was concluded that the observed differences were due to the superposition of tautomers, considering the dynamic disorder nature in TAE crystals.[5] According to their study, the strength of intermolecular interactions decreases with temperature. The ordering of the crystal structure at 110 K resulted from the rise of the barrier proton transfer.[5] The hydrogen-bonded proton was found to migrate from the central position at 298 K closer to one of the oxygen atoms at 110 K.

A variable temperature (VT) neutron diffraction study at five temperatures between 20 K and 298 K allowed a more accurate characterization of the migrating proton.[6] With the exception of the intramolecular hydrogen bond, the overall molecular structure was identical at five temperatures and consistent with previous reports. With the decrease in temperature, the O2-H distance decreased from 1.171(11) Å to 1.081(2) Å and the O1-H distance increased from 1.327(10) Å to 1.416(2) Å (Figure 6). Over the temperature range 20 K to 298 K, the enolic hydrogen appeared to be closer to O2 (see Figure 6).

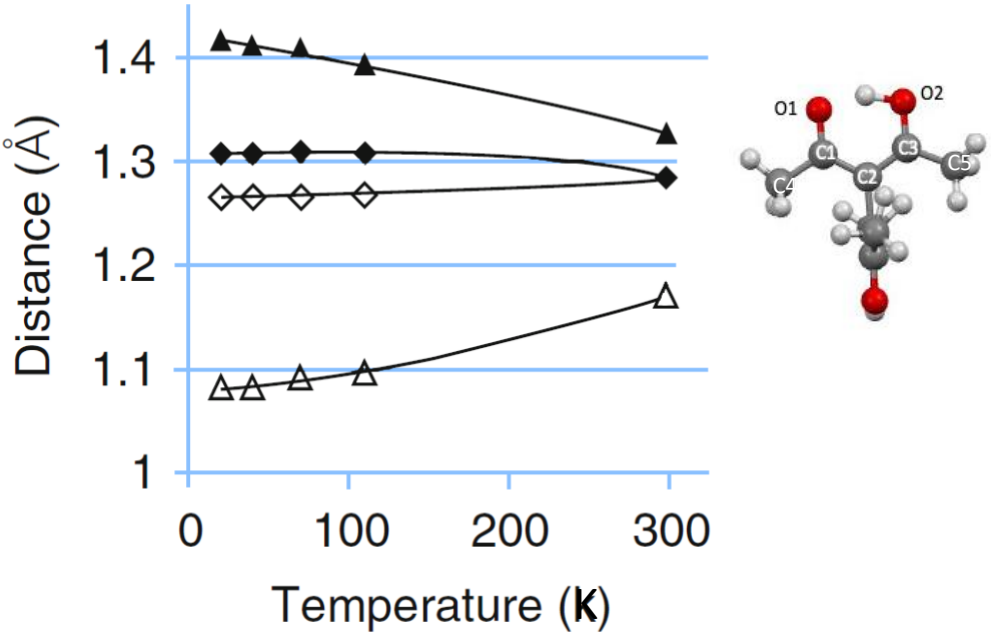

Figure 6. Atom-atom separation in TAE as a function of temperature. H1 denotes the enolic hydrogen. Empty triangles denote H1-O2 bond length, empty diamonds O1-C1, black diamons O2-C3 and black triangles H1-O1.[6]

2. Compounds Studied

2.1. Tetraacetylethane

Figure 6 clearly illustrates hydrogen migration path. With increasing temperature, H1 moves further away from O2 and closer to O1. At the same time, the decrease in O2-C3 distance indicates the bond acquires more double-bond character and the O1-C1 becomes more similar in nature to a single bond. The authors note that the convergence of both C-O bonds at 298 K can be explained by the resonance assisted hydrogen bond model. [1,5]

Periodic density functional quantum calculations provided in this study reproduce the geometry of hydrogen bond at low temperatures.[6] The authors propose that hydrogen migration towards the center with increasing temperature may be due to increased vibrational amplitude of the proton and that the potential energy well is asymmetric.

In conclusion, the structure of TAE has been extensively analyzed by X-ray and neutron diffraction. In general, neutron diffraction and later X-ray diffraction studies confirm the asymmetric nature of the intramolecular hydrogen bond and temperature dependence of the enolic hydrogen position. The availability of reliable crystal structures offers the advantage of using TAE as the first model compound presented in this thesis in terms of measuring deuterium isotope effects on ^{13}C chemical shifts and the information that can be extracted with the use of solid-state NMR, presented in the next sections.

2.1.2. Deuterium Isotope Effects on ^{13}C NMR Chemical Shifts at Room Temperature

i) Experimental Methods

In all solid-state spectra NMR presented in this work, the uncertainty in the chemical shifts is approximately 0.02 ppm. Solid-state 1,1,2,2-tetraacetylethane and all solvents were purchased from Sigma Aldrich.

TAE-OD: To prepare deuterium labelled TAE, approximately 4 mL of methanol-OD was added to 0.404 mmol of TAE crystals and the sample was shaken. Approximately 4 mL of chloroform-*d* was added to the mixture to dissolve the remaining solid. The solution was left in an open 10 mL glass vial for slow evaporation at room temperature. Solid TAE-OD was collected after 48 hours.

Solid-state NMR: Solid-state ^{13}C NMR spectra were obtained at 11.75 T using a Bruker Avance NEO 500 NMR spectrometer operating at 125.8 MHz for ^{13}C and 500.1 MHz for ^{1}H, with a Bruker 4 mm probe operating in double-resonance mode. All data were acquired under magic-angle spinning (MAS) conditions at a spinning frequency of up to 14 kHz using the cross-polarization (CP) technique with a 62.5 kHz ^{1}H decoupling field. The ^{1}H 90° pulse was 4.0 µs and the contact time was 3 ms; 3492 to 4152 transients were co-added for each spectrum.

2. Compounds Studied

2.1. Tetraacetylethane

ii) Results and Discussion

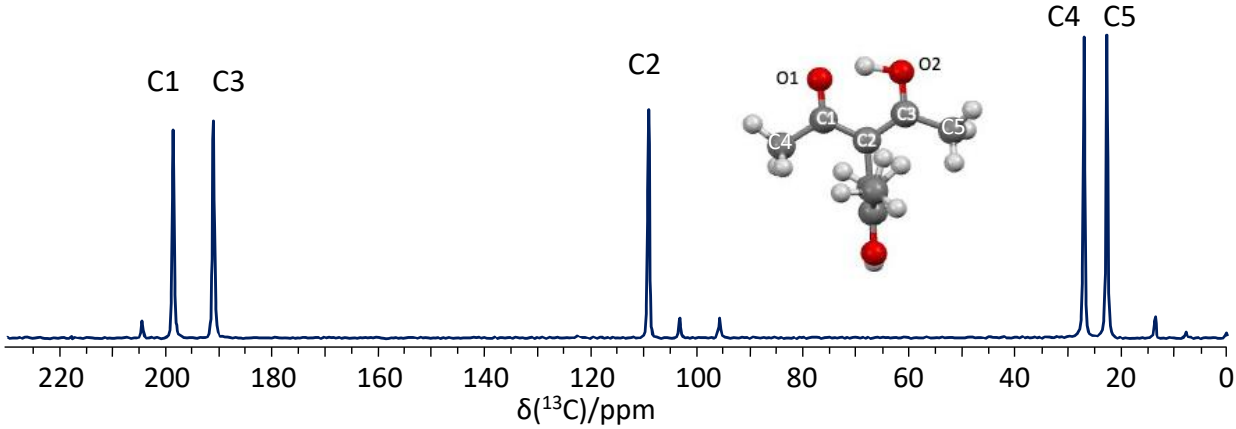

Figure 7. C-13 NMR spectrum of natural abundance TAE in the solid state. Acquired at 11.75 T and 293 K, with spinning frequency of 12 kHz. The low intensity peaks are the spinning sidebands.

The spectrum in Figure 6 shows three sets of peaks in natural abundance TAE. The two most downfield peaks at approximately 200 ppm and 193 ppm arise due to C1 and C3 carbons, while the single peak at about 110 ppm is assigned to C2. It is worth noting that in the solid state we can not only distinguish between C1 and C3, but also between the two methyl groups in the 20-30 ppm range. In comparison with acac, in which only one peak is observed at 191.25 ppm and C1/C3 atoms are equivalent and slightly more shielded.

Upon deuteration of the enolic hydrogen, the appearance of the ^{13}C NMR spectrum changes, as shown in Figure 8.

2. Compounds Studied

2.1. Tetraacetylethane

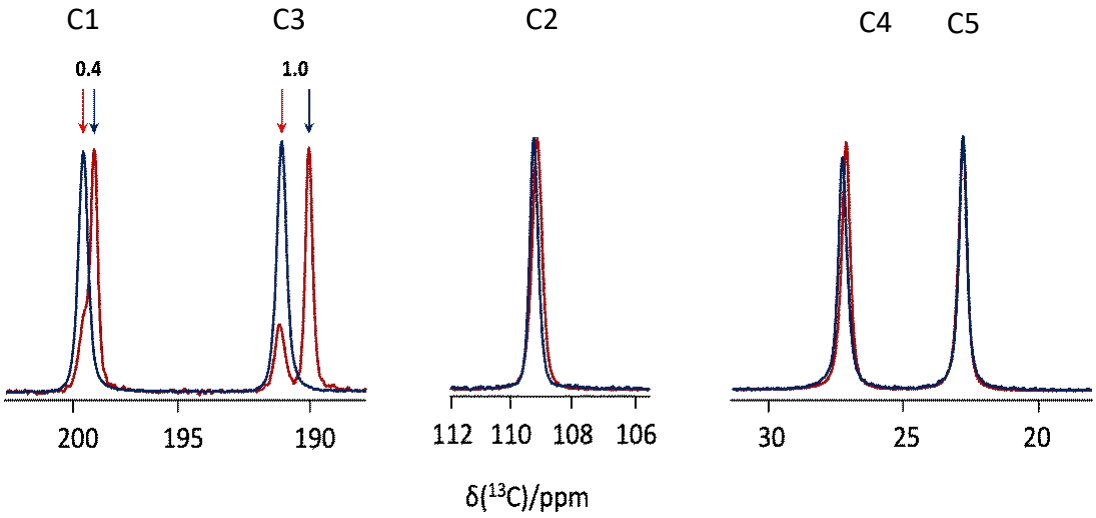

Figure 8. Enlarged parts of the ^{13}C NMR spectra of natural abundance TAE (dark blue) and TAE-OD (red).

Figure 8 depicts the effect of substituting the enolic hydrogen for deuterium on the ^{13}C NMR chemical shifts. The most significant difference can be observed in peaks corresponding to C1 and C3 atoms. A small deuterium isotope shift of 0.4 ppm affects C1, while C3 experiences a more significant shift of 1.0 ppm. The lower intensity peak at approximately 193 ppm in the deuterated compound (red trace) is due to partially unlabeled compound. The C2 nucleus experience a small isotope effect, similarly to one of the methyl carbons (C4).

As mentioned in the introduction, upon substitution by heavier atom, other NMR resonant nuclear experience change in rovibrational averaging of electronic properties, thus the change in the chemical shifts.[7] The reason behind the effect isotope labelling has on electronic properties, kinetics, and equilibrium properties, is the anharmonicity of the potential energy well. For any vibrational state, the energy of the species labelled with heavier isotope, is lower than the energy of the natural abundance system. This results in a shorter average bond length in the compound labelled with heavier isotope and is referred to as intrinsic isotope effect.[7]

2. Compounds Studied

2.1. Tetraacetylethane

The most significant deuterium isotope shift of 1.0 ppm affects the ^{13}C NMR peak corresponding to C3. As C3 is bonded to O2, it can be concluded that the distance between D-O2 atoms is shorter than between D-O1 and deuterium is moving towards O2. The hydrogen bond is clearly asymmetric and hydrogen atom favors position closer to the O2.

This conclusion is consistent with previously published experimental neutron diffraction data and illustrates the feasibility of measuring isotope effects on NMR chemical shifts as a complementary method of intramolecular hydrogen bond characterization in the solid state.

2.1.3. Deuterium Isotope Effects on ^{13}C NMR Chemical Shifts at Variable Temperature

i) Experimental Methods

Variable Temperature NMR:

Variable-temperature ^{13}C NMR spectra were acquired with CP conditions described in the previous experimental section in the 163 to 342 K region with MAS frequency of 5 kHz using the Bruker BSVT system supplied with the instrument. 164 to 300 transients were co-added to each spectrum. Low temperatures were achieved by using $N_{2(liq)}$ as the heat exchange source N_2 boiloff gas was used as an ultra-dry VT gas source. Temperatures were calibrated based on the temperature dependence of ^{207}Pb chemical shift of methylammonium lead iodide, as recently reported.[68] The uncertainty of this approach is estimated to be < ±2 K.

ii) Results and Discussion

In case of the variable temperature NMR experiments (VT NMR) on TAE, there are two contributions to the observed isotope shift: the intrinsic isotope effect due to the presence of a heavier nucleus denoted as Δ_o and perturbation of the equilibrium Δ_{eq} (Eq. 3).[57]

2. Compounds Studied

2.1. Tetraacetylethane

Equation (3) $$\Delta_{obs} = \Delta_o + \Delta_{eq}$$

The intrinsic isotope effect arises from the difference in the ground vibrational state of the O-H and O-D bonds as illustrated in Figure 9. For any vibrational state, the energy of the species labelled with heavier isotope, is lower than the energy of the natural abundance system. This results in a shorter average bond length in the compound labelled with heavier isotope. Therefore, the measurement of the isotope effect provides information about the potential energy surfaces.[7] This arises from the fact that the proton in an intramolecular hydrogen bonding becomes more deshielded as it moves toward the midpoint between the heavy atoms, such as O.[7] Potential energy surface of many hydrogen bonds has two inequivalent minima, i.e., they are asymmetric double wells.[69] The three, less common symmetric potential energy well shapes are illustrated in the work by Forsén et al. summarized in Figure 9.

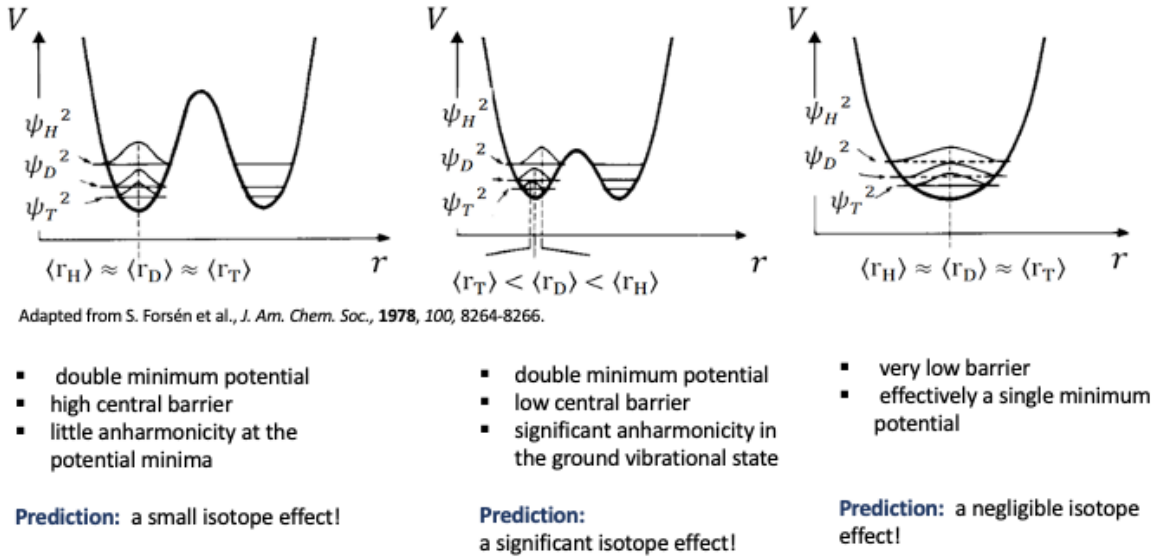

Figure 9. Illustration of the position of hydrogen isotopes for different types of symmetric potential functions, in the zero-point vibrational levels and predicted isotope effect.[7]

2. Compounds Studied

2.1. Tetraacetylethane

When a system, such as TAE exists in different tautomeric forms, presence of deuterium rather than a hydrogen atom causes changes in the tautomeric equilibrium. Changes in the chemical equilibrium can occur along with the equilibrium isotope effect.[50,70]

This information is crucial in explaining the results of VT ^{13}C NMR experiments on TAE which are presented in Figure 10. The values of ^{13}C NMR chemical shifts at three different temperatures are summarized in Table 1.

Table 1. Summary of ^{13}C NMR chemical shifts of TAE and TAE-OD at variable temperature.

TAE	$\delta(^{13}C)$/ppm ± 0.1				
Temperature/ K	C1	C3	C2	C4	C5
163	201.6	188.2	108.0	28.1	21.1
294	198.9	190.9	109.0	27.2	22.7
342	198.0	191.4	109.3	26.9	23.0
TAE-OD					
163	202.0	185.8	108.2	28.6	20.8
294	198.5	189.8	109.1	27.3	22.6
342	197.6	190.6	109.5	27.0	23.1

2. Compounds Studied

2.1. Tetraacetylethane

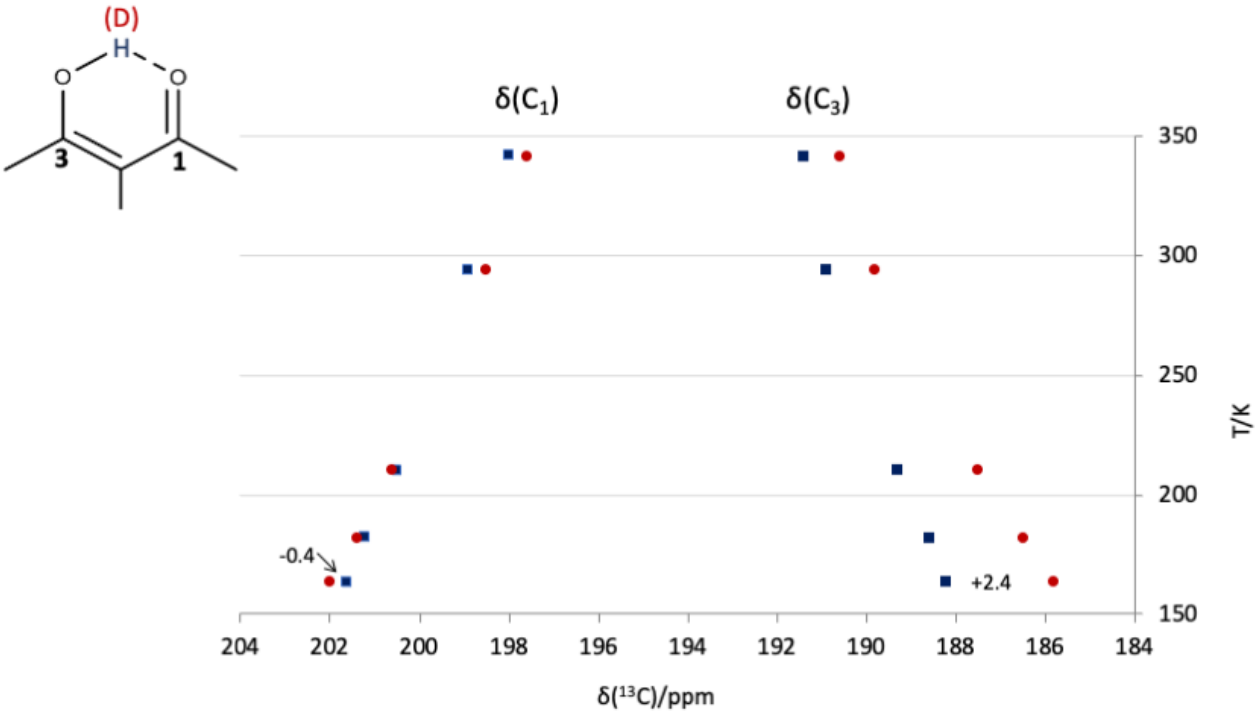

Figure 10. Temparature dependence of ^{13}C NMR chemical shifts of nuclei C1 and C3 in TAE and TAE-OD.

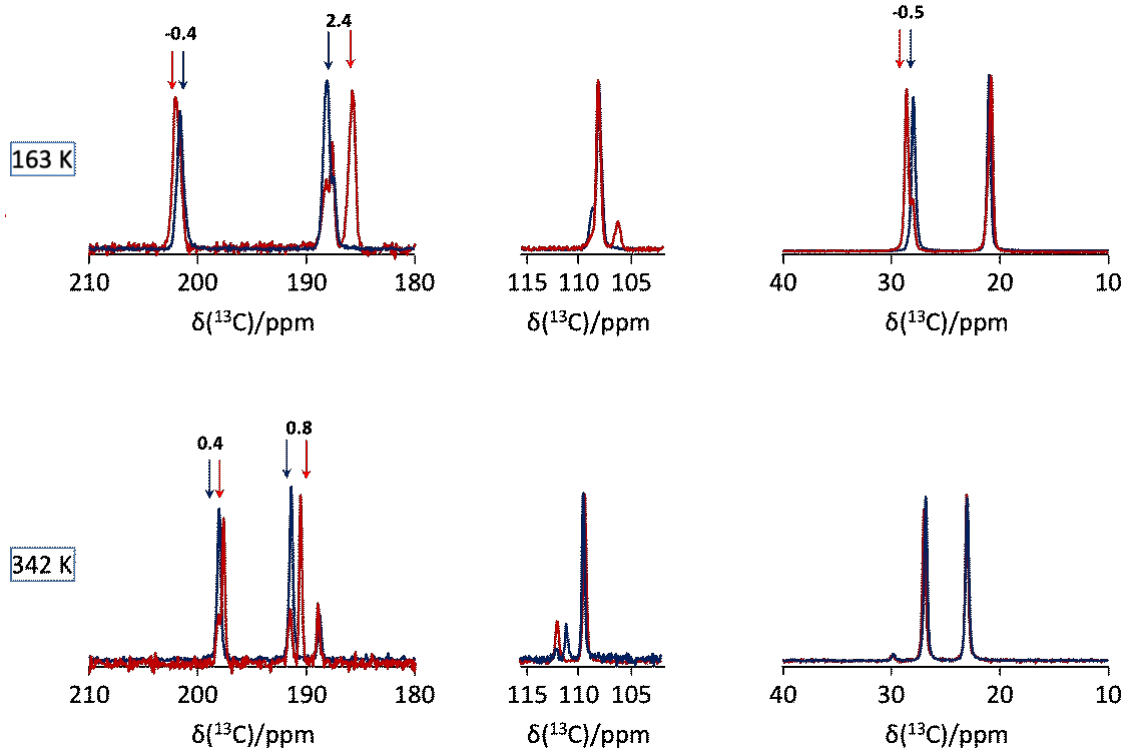

Figure 11. Enlarged parts of the ^{13}C NMR spectra of natural abundance TAE (dark blue) and TAE-OD at 163 K and 342 K. Acquired at 11.75 T with the spinning frequency of 5 kHz.

Similar to the spectra acquired at room temperature, the deuterium isotope shift is more significant for C3 than C1 at 163 K and 342 K, further supporting the finding that deuterium favours O2 and the hydrogen bond is asymmetric. The most significant deuterium isotope shift of 2.4 ppm is observed at 163 K at C3. As the temperature decreases, deuterium atom moves closer to O2. At the same time, C1 nucleus experiences the isotope shift of -0.4 ppm and is becoming more deshielded when deuterium replaces hydrogen. Although considering only the principles of the intrinsic isotope shift, the C1 peak should become more shielded upon deuteration, one must consider the contribution of the equilibrium isotope shift, Δ_{eq}. Large peak separation in similar hydrogen-bonded systems, such as those consisting of asymmetric tautomers (malonaldehyde, 3-hydroxy-2-phenylpropenal) has been observed at low temperatures in solution and was attributed to the perturbation of an equilibrium between the two tautomers.[57] The same phenomenon applies to the solid state, where lowering the temperature introduces more imbalance in the equilibrium, and presence of a distinct tautomer is more prevalent. In case of TAE, the isotope shift of the significant 2.4 ppm magnitude temperature arises due to the change in the equilibrium caused by significantly lower temperature.

The smallest deuterium isotope shift of C3 appears at 342 K. C3 is still the most affected nucleus, indicating the preference of hydrogen to be closer to O2. As the temperature increases, the magnitude of deuterium isotope shift of C3 decreases, suggesting the temperature dependence of the hydrogen position. The O1-O2 separation decreases at higher temperature and H-O2 bond length increases, as indicated in the neutron diffraction study.[6,61] It can be concluded, that with the increase in temperature, hydrogen changes position towards the center of the hydrogen bond, but the bond does not become completely symmetric, as suggested in the first X-ray diffraction study.[58]

2. Compounds Studied

2.1. Tetraacetylethane

iii) Conclusions

Deuterium isotope effects on ^{13}C chemical shifts of tetraacetylethane confirm the asymmetric nature of the intramolecular hydrogen bond. Both room temperature and VT studies indicate the preference of the hydrogen atom to be in proximity to O2. Moreover, the magnitude of deuterium isotope shifts is temperature dependent, and the enolic hydrogen is located further away from O2 at higher temperatures. These findings are consistent with variable temperature neutron diffraction studies.[6] Since the structures obtained by neutron diffraction are among the most reliable in determination of hydrogen atom position, the consistency of results obtained by measuring deuterium isotope effect on ^{13}C NMR chemical shifts proves that NMR studies in the solid-state are a reliable method to characterize the nature of intramolecular hydrogen bonding.

2.2.1. Avobenzone Applications and Importance

The use of sunscreens – chemicals that absorb, reflect or scatter UV radiation, is a simple precaution that helps to decrease the negative impact of UVR exposure, preventing diseases such as skin carcinomas and malignant melanomas. However, the most recent report of the American Food and Drug Administration demonstrates that active sunscreen ingredients are systematically absorbed through skin into blood plasma, likely accumulating in organs, causing endocrinal disruption and gDNA damage.[71] Moreover, these are environmental contaminants of substantial concern, with up to 14,000 tons of sunscreens being released into oceans every year.[72] In the light of these reports, understanding the properties of sunscreen ingredients on molecular level is of significant importance. In this context, hydrogen bonding is among the very influential properties affecting factors like solubility and bioavailability of sunscreen components.

Avobenzone, or 3-(4-tert-Butylphenyl)-3-hydroxy-1-(4-methoxyphenyl)-2-propen-1-one, is one of the most used organic UVA filters and is a 1,3-diketone that presents an example of keto-enol tautomerism.[73] These features, along with the asymmetric nature of its molecule (two different functional groups on the phenyl rings), makes avobenzone a suitable model compound to investigate the nature of its hydrogen bonding, that can provide information useful in direct drug research.

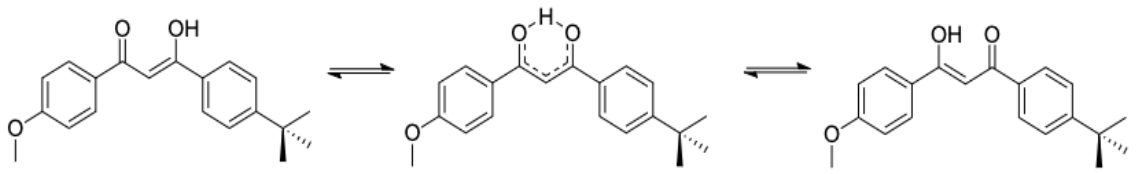

Figure 12. Keto-enol tautomers of avobenzone.

2.2.2. Crystal Structure

To date, one X-ray diffraction structure of avobenzone has been reported.[8] It was recrystallized from acetonitrile and the structure was obtained at room temperature. The analysis of C-C and C-O bond distances as well as O---O separation in the carbonyl region of the molecule suggested an enol structure with the enolic hydrogen atom position being closer to the *tert*-butyl side of the molecule. Moreover, the *tert*-butyl group of avobenzone was disordered and two types of *tert*-butyl groups were observed with site occupancies ratio 1:1, as presented in Figure 13.

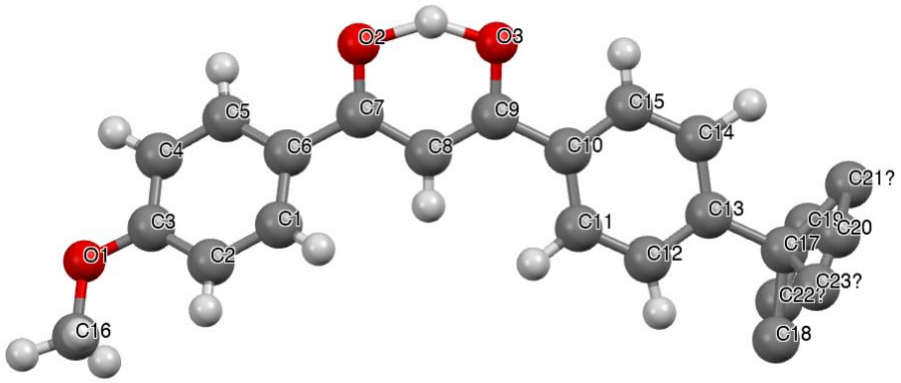

Figure 13. X-ray structure of avobenzone molecule with disordered *tert*-butyl group.[8]

2.2.3. ^{13}C NMR Spectrum Assignment of Avobenzone in the Solid State

i) Experimental Methods

Solid-state avobenzone and all solvents were purchased from Sigma Aldrich.

Solid-state NMR: Solid-state ^{13}C NMR spectra were obtained at 11.75 T using a Bruker Avance NEO 500 NMR spectrometer operating at 125.8 MHz for ^{13}C and 500.1 MHz for ^{1}H, with a Bruker 4 mm probe operating in double-resonance mode. All data were acquired under magic-angle spinning (MAS) conditions at a spinning frequency of up to 14 kHz using the cross-

polarization (CP) technique with a 62.5 kHz ^{1}H decoupling field. The ^{1}H 90° pulse was 2.5 µs and the contact time was 3 ms; 208 to 4664 transients were co-added for each spectrum.

ii) Results and Discussion

Initially, a ^{13}C NMR spectrum of natural abundance avobenzone was acquired at room temperature. The peak assignment is presented in Figure 11. Peaks were assigned based on the ^{13}C NMR data published in the literature.[73,74] Some peaks, which were difficult to assign, especially in the aromatic region, were determined with the help of solution NMR experiments (Appendix A).

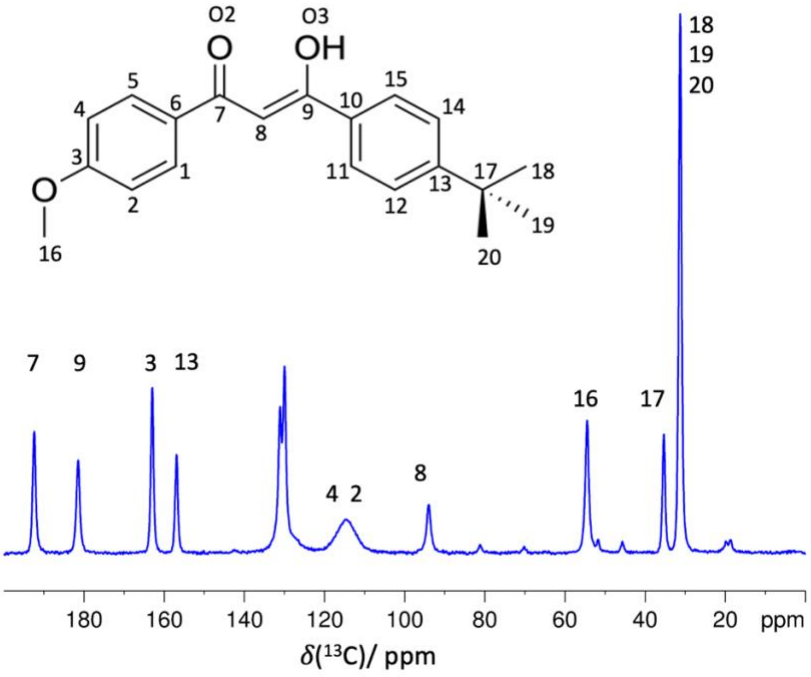

Figure 14. C-13 NMR spectra of natural abundance avobenzone at 303 K. Acquired at 11.75 T with the spinning frequency of 5 kHz.

2.2.4. Deuterium Isotope Effects on ^{13}C NMR Chemical Shifts at Room Temperature

i) Experimental Methods

Avobenzone-OD: To prepare deuterium labelled avobenzone, approximately 4 mL of methanol-OD was added to 0.404 mmol of avobenzone powder and the sample was shaken. Approximately 4 mL of chloroform-*d* was added to the mixture to dissolve the remaining solid. The solution was left in an open 10 mL glass vial for slow evaporation at room temperature. Solid avobenzone-OD was collected after 48 hours.

Solid-state NMR: Solid-state ^{13}C NMR spectra were obtained at 11.75 T using a Bruker Avance NEO 500 NMR spectrometer operating at 125.8 MHz for ^{13}C and 500.1 MHz for ^{1}H, with a Bruker 4 mm probe operating in double-resonance mode. All data were acquired under magic-angle spinning (MAS) conditions at a spinning frequency of up to14 kHz using the cross-polarization (CP) technique with a 62.5 kHz ^{1}H decoupling field. The ^{1}H 90° pulse was 2.5 µs and the contact time was 3 ms; 1820 to 4664 transients were co-added for each spectrum.

ii) Results and Discussion

Upon deuteration of the enolic hydrogen, the appearance of the ^{13}C NMR spectrum changes, as shown in Figure 15.

2. Compounds Studied

2.2. Avobenzone

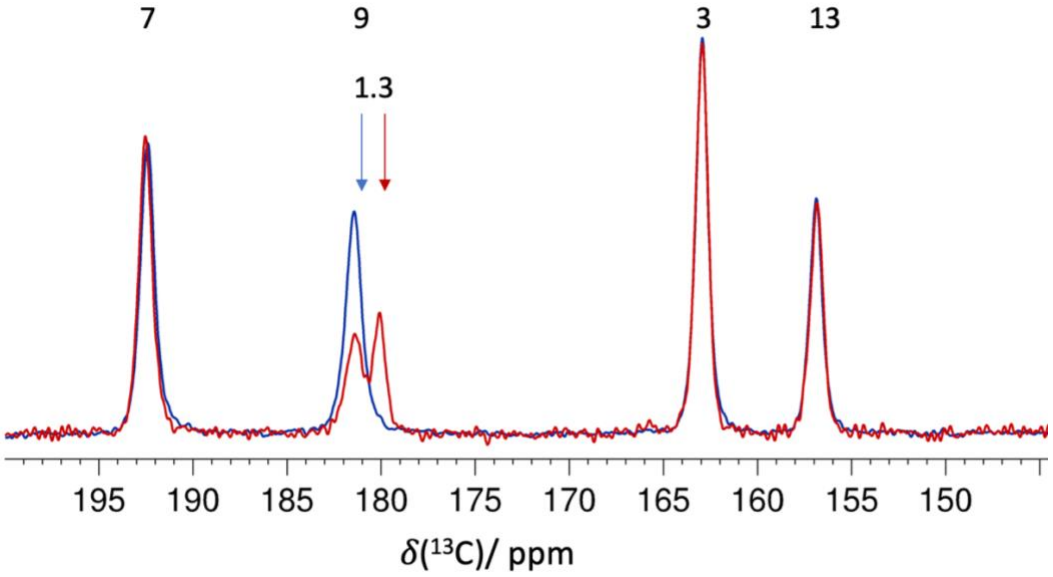

Figure 15. Enlarged part of the ^{13}C NMR spectrum of natural abundance avobenzone (dark blue) and avobenzone-OD (red). Acquired at 11.75 T with the spinning frequency of 5 kHz at room temperature.

As it can be seen in Figure 15, the carbon nucleus affected the most by the deuterium isotope shift is C9. At room temperature, the C9 chemical shift experience an isotope effect of 1.3 ppm, making the C9 more shielded in the presence of deuterium. The rest of the peaks in the 200-150 ppm range are essentially unaffected. Since C9 is the nucleus experiencing the major change upon deuterium substitution, it indicates the preference of the enolic H/D to spend more time in closer proximity to O3. As explained in the previous chapter, this intrinsic isotope effect is a result of a substitution with heavier nucleus (deuterium), causing the shorter average O-D bond length and lower energy of the vibrational states comparing with the natural abundance system.

The analysis of X-ray structure interatomic distances is consistent with this finding.[8] Although the X-ray structure was obtained at room temperature, and in general, X-ray diffraction is not a reliable method of determination of hydrogen position, it is still worth to analyze the interatomic distances in the keto-enol fragment of the molecule. The C8-C9 distance of

1.365(9) Å is shorter than C7-C8 bond length of 1.41(1) Å, suggesting that C8-C9 bond has more double-bond character. Comparing the two C-O distances, C7-O2 distance of 1.264(7) Å is shorter than C9-O3, which is 1.318(6) Å. The O3-H distance of 1.240 Å is shorter than 1.358 Å of O2-H. Overall, the bond lengths within the keto-enol fragment of avobenzone, similarly to TAE are consistent with the resonance-assisted hydrogen bonding model[1] and indicate an asymmetric intramolecular hydrogen bonding with enolic hydrogen atom being closer to O3.

Some computational studies providing the structure of the enol tautomer of avobenzone are available in the literature.[75,76] In their first publication, the authors claim the position of the enolic hydrogen to be in proximity to the side of the molecule with the methoxybenzene ring.[76] In the following article, the published absolute enthalpies for the two enol forms (one with H closer to O2 and the other with H closer to O3) are very similar with insignificant difference.[75]

The disagreement between the published computational results and experimental results obtained in this thesis arises mainly because the computations used DFT and modeled an isolated avobenzone molecule in the gas phase. It illustrates the efficacy of NMR spectroscopy and measuring deuterium isotope effects as a viable experimental method of determination the position of the enolic hydrogen in intramolecular hydrogen bonding for compounds in the solid state.

2.2.5. Deuterium Isotope Effects on ^{13}C NMR Chemical Shifts at Variable Temperature

i) Experimental Methods

Variable Temperature NMR: Variable-temperature ^{13}C NMR spectra were acquired with CP conditions described in the previous experimental section in the 163 to 342 K region with MAS frequency of 5 kHz using the Bruker BSVT system supplied with the instrument. 208 to 1194

transients were co-added to each spectrum. Low temperatures were achieved by using N_2(liq) as the heat exchange source N_2 boiloff gas was used as an ultra-dry VT gas source. Temperatures were calibrated based on the temperature dependence of ^{207}Pb chemical shifts of methylammonium lead iodide, as recently reported.[68]

ii) Results and Discussion

C-13 NMR spectra of avobenzone-OD at 212, 301 and 346 K are shown in Figure 16.

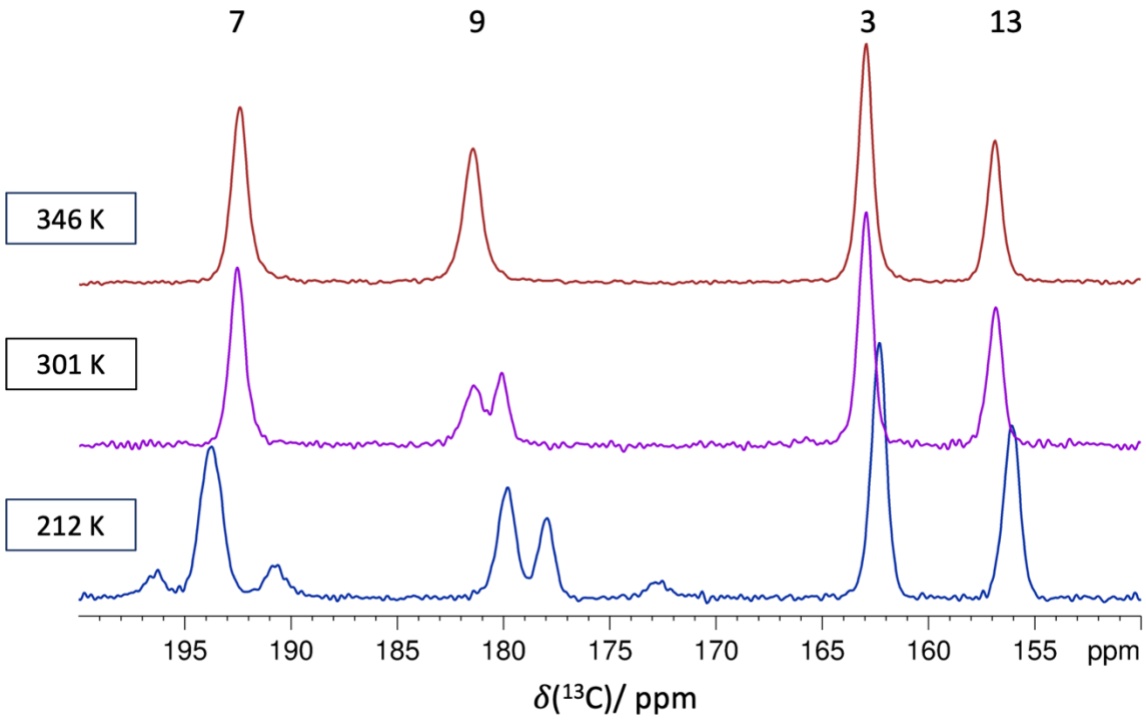

Figure 16. Fragment of the ^{13}C NMR spectrum of solid-state avobenzone-OD at variable temperature. Acquired at 11.75 T with the spinning frequency of 9 and 10 kHz.

Focusing on the carbonyl/enolic carbon peaks for C7 and C9, there is a clear chemical shift temperature dependence. While C7 and C9 have chemical shifts of 192.72 ppm and 179.76 ppm at room temperature, respectively, a clear isotope effect occurs with the change in temperature. The exact values of ^{13}C NMR chemical shifts are reported in Table 2. The presence of two peaks assigned as C9 at 212 K and 301 K arises from a mixture of natural abundance and deuterium

labelled avobenzone in the bulk sample. Peak from avobenzone-OD sample is the more shielded of the pair.

Table 2. Summary of ^{13}C NMR chemical shifts of avobenzone and avobenzone-OD at variable temperature.

Avobenzone	δ(^{13}C)/ppm	±	0.1	ppm					
Temperature/ K	C7	C9	C3	C13	C2 C4	C8	C16	C17	C18, 19, 20
303	192.40	181.44	162.94	156.88	114.70	93.95	54.42	35.26	31.18
Avobenzone-OD									
346	192.13	180.67	163.09	157.00	114.65	93.91	54.55	35.36	31.31
301	192.72	179.76	162.83	156.72	117.34 111.80	93.74	54.30	35.20	31.09
212	193.74	179.81	177.95	156.09	116.87 111.18	93.40	53.83	34.89	30.67

2. Compounds Studied

2.2. Avobenzone

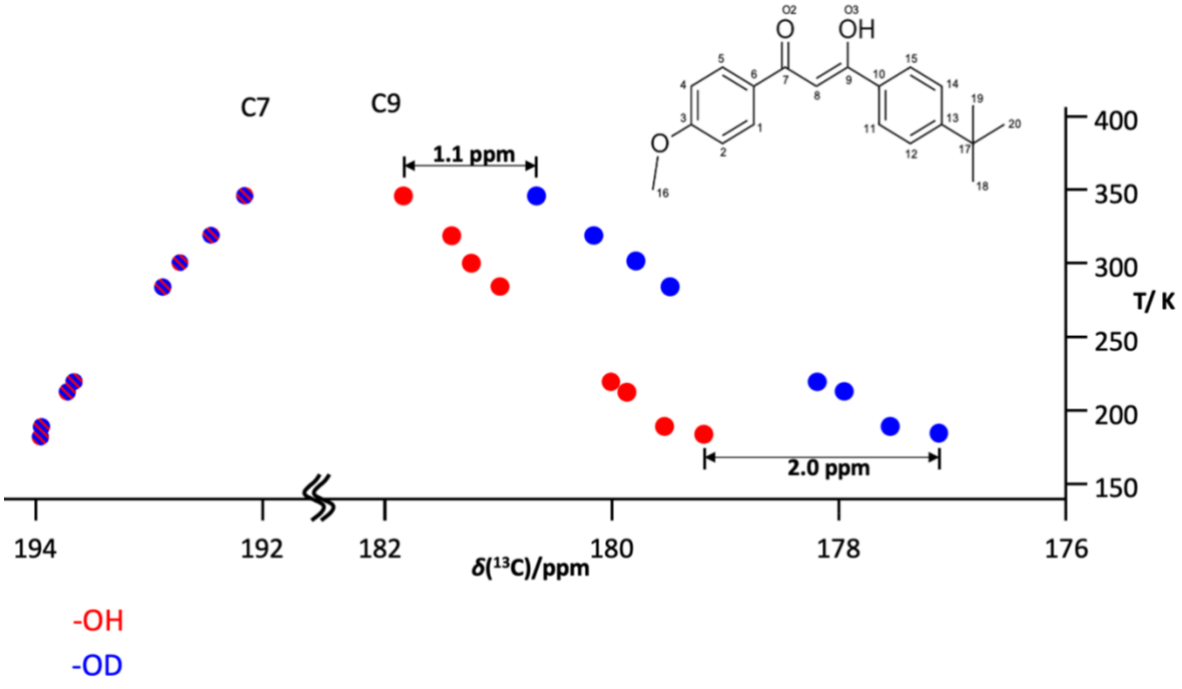

Figure 17. Temperature dependence of ^{13}C NMR chemical shifts of nuclei C7 and C9 in avobenzone and avobenzone-OD.

The deuterium substitution and the decrease in temperature affects C9 nucleus more than C7. A deuterium isotope shift of a 2.0 ppm magnitude is not only due to the intrinsic isotope effect but is possible because of a contribution from the equilibrium isotope effect described in the previous sections. The VT ^{13}C NMR experiments confirm the initial finding from RT isotope effect measurements: C9 is the nucleus mostly affected by the substitution of enolic hydrogen with deuterium, therefore it can be concluded that the enolic proton preferred position is on O3. With the decrease in temperature deuterium atom moves closer to O3, while it moves towards the center of the hydrogen bond at higher temperature, similarly to what was observed in TAE. Also, as in case of TAE, the enolic proton never reaches the center of the bond and the geometry of the intramolecular hydrogen bond remains asymmetric at all temperatures.

2.2.6. Molecular Motion in Avobenzone Crystals

Molecular motion of compounds like proteins has been of interest in the scientific community, due to its role in catalysis, function, enzymatic properties, and their behavior in cellular membranes.[77–79] Solution NMR has been a classic method of protein dynamics timescale determination.[80,81] Although studying solid proteins has gained more attention relatively recently, solid-state NMR has allowed an array of insights about structural and dynamic nature of investigated biomolecules.[82–86]

In case of the dynamics of smaller aromatic molecules, two studies are of particular interest. In their work, Li and McDermott found a millisecond aromatic ring flip motion in L-phenylalanine hydrochloride crystals, using solid-state NMR.[87] Another work presented the fast isotropic rotation in the crystal defect of imidazolium ion above 263 K.[88]

In the course of our studies of avobenzone it was found that the appearance of the ^{13}C NMR spectra were temperature dependent. Variable temperature ^{13}C experiments showed the obvious presence of a two-site exchange process, described in the sections below.

i) Results and Discussion

The appearance of the ^{13}C NMR spectra of avobenzone-OD at three different temperatures is shown in Figure 18.

2. Compounds Studied

2.2. Avobenzone

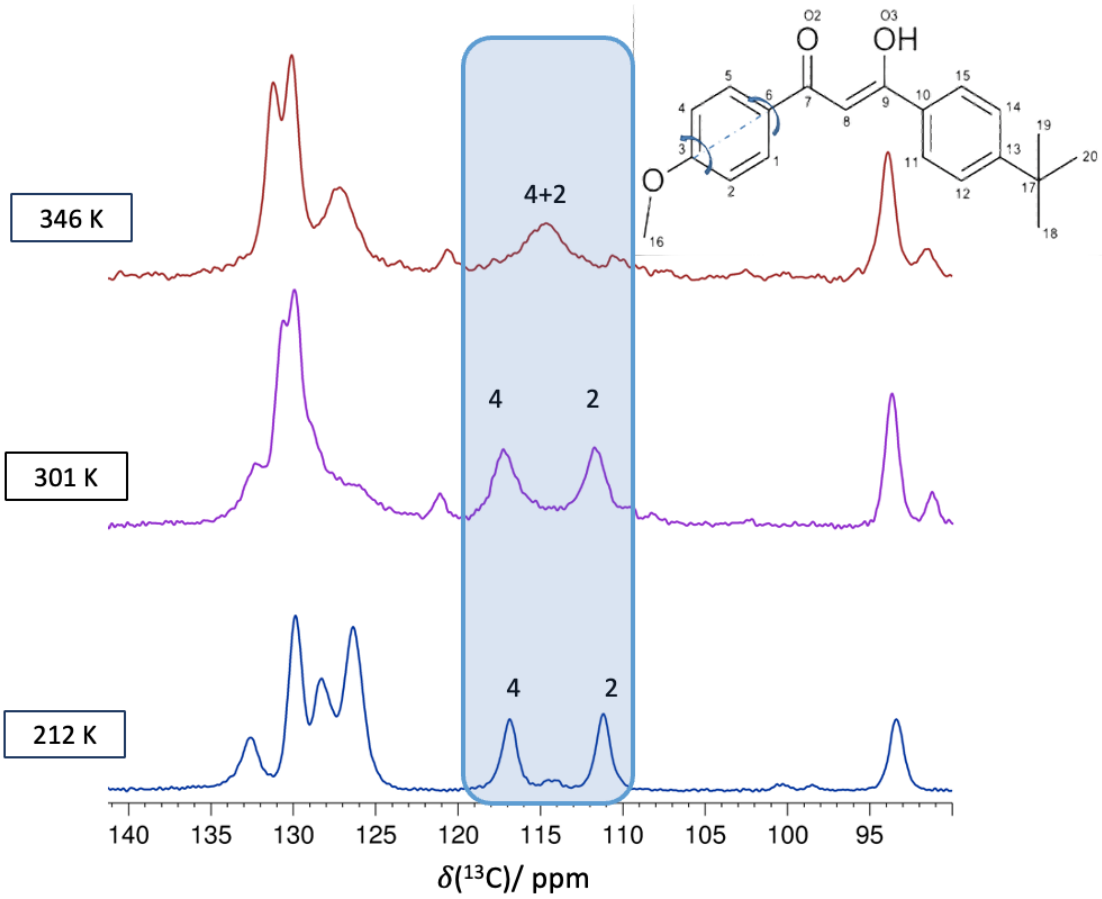

Figure 18. Aromatic region of the ^{13}C NMR spectrum of avobenzone-OD at 212, 301 and 346 K. Acquired at 11.75 T with the spinning frequency of 9 and 10 kHz.

A temperature-dependent change of peaks corresponding to carbon atoms C2 and C4 suggest a dynamic motion in solid-state avobenzone. It was possible to determine that C4 is the more deshielded of the C2/C4 pair, based on the NMR studies of anisole and other 1,4-disubstituted benzenes in the solid state.[89,90] At low temperature of 212 K the two peaks are clearly separate with two very different chemical shifts of 116.87 ppm and 111.18 ppm. With the increase in temperature, the two peaks become broader, and finally coalesce into one peak at 114.65 ppm, a value very close to the average of the two low temperature chemical shifts. A series of VT experiments allowed to establish a coalescence temperature of approximately 309 ± 2 K.

As for the appearance of the aromatic region 120-140 ppm in Figure 17, solution NMR experiments were conducted to assign the aromatic carbon peaks (Appendix A). However, the complex and changing appearance of the temperature-dependent spectra in the solid state does not allow appropriate peak assignments. The broad and changing nature of these peaks suggest temperature-dependent dynamic changes affecting carbon nuclei on the phenyl rings.

Rate and Barrier of the Methoxybenzene Ring Flips

For a simple two-site exchange A ⇌ X, the lifetime of a nucleus is equal at site A and X and is denoted as τ^c.[91]

At coalescence, the rate constant *k* can be expressed by Equation 4.

Equation (4) $$k = \frac{1}{\tau^c} = \pi \frac{\nu_A - \nu_X}{\sqrt{2}}$$

where ($\nu_A - \nu_X$) is the chemical shift difference between site A and site X, in Hz in the absence of exchange. For avobenzone in the solid state at 11.75 T,

$\nu_A - \nu_X$ = 717 Hz ± 10 Hz

Equation (5) $$k = \pi \frac{717 s^{-1}}{\sqrt{2}} = 1593\ s^{-1} \pm\ 22 s^{-1}$$

It is possible to estimate the free energy of activation using Equation 6,

Equation (6) $$k = \kappa \left(\frac{k_B T}{h}\right) \exp\left(\frac{-\Delta G\dagger}{RT}\right)$$

where κ is a transmission coefficient, generally taken as unity, k_B is the Boltzmann constant, h is the Planck constant, R is the molar gas constant and T is the absolute temperature at coalescence. Substituting numerical values for avobenzone, we obtain:

Equation (7)

$$1593\ s^{-1} \pm\ 22 s^{-1} = 1.0 \text{ x } \frac{1.381 \text{ x } 10^{-23} \text{ J } K^{-1}\ (309 \pm 2\ K)}{6.626 \text{ x } 10^{-34} \text{ J s}} \exp\left(\frac{-\Delta G\ \dagger}{RT}\right)$$

$$1593\ s^{-1} = 6.439 \text{ x } 10^{12} s^{-1} \exp\left(\frac{-\Delta G\ \dagger}{RT}\right)$$

$$\exp\left(\frac{-\Delta G\ \dagger}{RT}\right) = 2.474 \text{ x } 10^{-10}$$

$$\frac{-\Delta G\ \dagger}{RT} = -22.12$$

$$-\Delta G\ \dagger = (-22.12) \text{ x } (8.314 \text{ J } mol^{-1}\ K^{-1}) \text{ x } (309 \text{ K})$$

$$\Delta G\ \dagger = 56.8 \text{ kJ } mol^{-1} \pm 1.6 \text{ kJ } mol^{-1}$$

Barriers between 20 and 100 kJ mol^{-1} can be investigated by variable temperature NMR.[92] To put the value of $\Delta G^{\dagger}$ for avobenzone ring flips into perspective, the barrier of rotation of ethane is approximately 12 kJ mol^{-1} and 74 kJ mol^{-1} for formamide. In case of cyclohexane ring flips the barrier is approximately 45 kJ mol^{-1}.[93–95]

ii) Conclusions

Temperature-dependent peak coalescence of carbons C4 and C2 indicates a dynamic ring flip in the methoxybenzene ring fragment of the avobenzone molecule. Knowing the difference in C4 and C2 signals at low temperature in the absence of exchange, it was possible to calculate the rate constant of the ring flip, resulting in a value of 1593 ± 22 s^{-1} at the coalescence temperature of 309 K. The barrier of this motion was found to be approximately 56.8 ± 1.6 kJ mol^{-1}.

3. Summary and Conclusions

Examples of the enolic forms of the 1,3-diketones and their deuterium-labelled equivalents presented in this work illustrate the following phenomena.

Measuring the deuterium isotope effect on ^{13}C NMR chemical shifts at room and variable temperatures indicates the asymmetric nature of intramolecular hydrogen bond in TAE. The available variable temperature neutron diffraction data – a gold standard in determination of the hydrogen atom position, shows agreement with findings obtained via solid-state NMR. The enolic hydrogen/deuterium atom changes position with varying temperature, however it never reaches the center of the hydrogen bond and remains asymmetric at all temperatures.

Similar nature of the hydrogen bond was observed in avobenzone. The deuterium isotope effect shows the preference of hydrogen to stay closer to the side of the molecule with *tert*-butyl group. Similarly, to TAE, the deuterium atom moves away from O3 with increasing temperature, but it never reaches the center of the hydrogen bond. The 2.0 ppm deuterium isotope shift observed in avobenzone at low temperature is of rare magnitude. It can be attributed to the contribution of the equilibrium isotope effect due to temperature change.

Moreover, the variable temperature NMR study of solid-state avobenzone showed that the appearance of the ^{13}C spectrum in the 110-120 ppm region is temperature dependent. The peaks in this region correspond to carbon atoms on the ring with -OCH_3 group, in the *meta* position. The increase of temperature causes broadening of otherwise two distinct peaks, and their coalescence at approximately 309 K (measured at 11.75 T). This is explained by a dynamic ring flip, occurring at the rate 1593 ± 22.21 s^{-1} in the solid state. The calculated free energy of activation of this movement was approximately 56.8 ± 1.6 kJ mol^{-1}.

Overall, the use of deuterium isotope effects on ^{13}C NMR shifts is a feasible method to characterize intramolecular hydrogen bonds in the enolic forms of solid-state 1,3-diketones and

beyond. It overcomes limitations posed by other methods (e.g., neutron and X-ray diffraction), as it does not require materials to be crystalline, nor the growth of single crystals is required. It is particularly useful when studying materials such as avobenzone, where their nature makes the crystal growth very challenging. Moreover, variable temperature experiments may uncover dynamic changes happening on a certain timescale, as illustrated by avobenzone ring flips.

4. Future Work

A natural extension of the work presented in this thesis includes expanding the pool of 1,3-diketones and measuring the deuterium isotope shifts in solid state. In the course of this program, it was possible to grow a single crystal and deuterium-label 3-hydroxy-1,3-bis(4-methoxyphenyl)propan-1-one, structure similar to avobenzone (Figure 19).

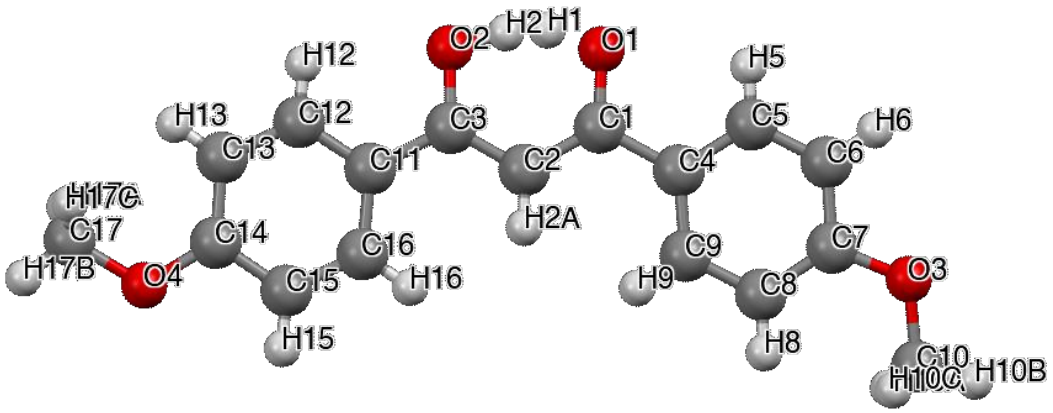

Figure 19. Molecule of 3-hydroxy-1,3-bis(4-methoxyphenyl)propan-1-one.

The depiction of hydrogen atoms H1 and H2 in this structure illustrates the hydroxyl-group hydrogen was disordered over two positions, each refined with an occupancy factor of 0.5.

The next step would involve acquiring ^{13}C NMR spectra of natural abundance and -OD labelled compounds at variable temperature. To date, spectra were collected at room temperature and are presented in Figure 20.

4. Future Work

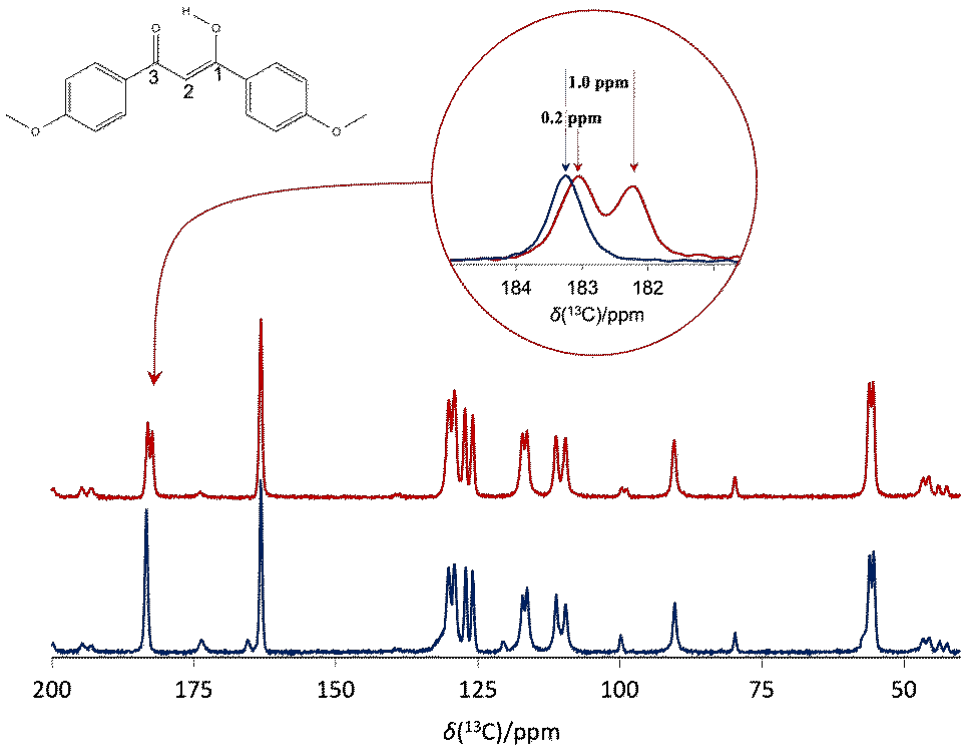

Figure 20. C-13 NMR spectrum of natural abundance 3-hydroxy-1,3-bis(4-methoxyphenyl)propan-1-one (dark blue) and 3-hydroxy-1,3-bis(4-methoxyphenyl)propan-1-one-OD (red). Acquired at 11.75 T with the spinning frequency of 5 kHz at room temperature.

The two most deshielded peaks in red and blue spectra are assigned as C3/C1. Upon deuteration of the enolic hydrogen, the most deshielded peak experiences deuterium isotope shift of 1.0 ppm, while the other peak at approximately 170 ppm remains unaffected. This indicates, that like in avobenzone, the enolic proton favors one side of the keto-enol molecule fragment over the other. This is a great illustration of the advantage of deuterium isotope effects on 13C chemical shifts as a method of hydrogen position determination. In contrast, X-ray diffraction study is unable to provide any insight regarding the position of the hydrogen in a disordered system.

The variable temperature NMR experiments can provide further insight into the structure of the compound. The presence and magnitude of deuterium isotope effect on ^{13}C chemical shifts of C1 and C3 will help to identify the position of enolic hydrogen, as well as indicate possible temperature dependent dynamic motions, such as ring flips like those observed in avobenzone.

Deuterium Isotope Labelling

Another extension of this work would involve developing alternative ways of deuterium labelling, using mechanochemistry, with a goal to reduce the volume of organic solvents used in the process.[96,97] Mechanochemistry has been used in O-17 and O-18 isotope labelling with success.[98] Nevertheless, the topic of mechanochemistry for deuterium labelling is not excessively present in the current literature.

Preliminary experiments involved mechanochemical deuterium labelling of avobenzone. Ball milling was used, with methanol-OD being the source of enolic deuterons. The independent variables included milling time (interval ranging from seconds to the maximum of 10 minutes) and the milling speed (3800 rpm and 4800 rpm). Results were verified by acquiring ^{1}H NMR spectra of the samples in $CDCl_3$ solution and the integration of the enolic hydrogen peak was indicative of the level of deuteration. The lowest -OH peak integration values were approximately 0.7, therefore an approximate 30% level of deuteration was deduced.

The major disadvantage of this approach was relying on solution NMR for sample screening. One would expect that once the sample is successfully labelled in the solid state, solution NMR would reflect the level of sample deuteration. However, the results prompt a speculation that there might be an exchange between avobenzone-OD and enolic hydrogen sources in solution (such as water contamination). The two main sources of water contamination are likely the NMR solvent and water used for cleaning the capsule used for milling. Despite leaving the capsule open after diligent wiping, the residual water is certainly trapped in the small pores inside the capsule.

The presence of water in the solution makes ^{1}H NMR unreliable in assessing the true level of deuteration achieved in the solid. Once water impurity is in the NMR solution, most

likely is an exchange with the enolic -OH of interest occurs. The most reliable sample screening method would involve ^{1}H and ^{2}H solid-state NMR, which was impractical due to the large number of samples.

Despite the possible exchange and disturbance caused by H_2O, it is still encouraging to see approximately 30% successful deuteration across the samples (regardless of the milling time and speed).

Possible changes in the experimental method to achieve higher deuteration level verified by a reliable method include:

- solvent drying; however, the residual water from the milling capsule will still most likely be present.
- heat-drying the milling capsule, however the maximum temperature would be determined by the temperature at which capsule material disintegrates.
- using higher sample concentration for ^{1}H solution NMR screening – the idea behind is that water molecules and avobenzone molecules compete to exchange the OH group; possibly, a significantly higher avobenzone concentration may supress the exchange with water in solution.

Bibliography

1. Gilli, G.; Bellucci, F.; Ferretti, V.; Bertolasi, V. Evidence for Resonance-Assisted Hydrogen Bonding from Crystal-Structure Correlations on the Enol Form of the β -Diketone Fragment. *Journal of the American Chemical Society* **1989**, *111* (3), 1023–1028.
2. Matlinska, M. A.; Wasylishen, R. E.; Bernard, G. M.; Terskikh, V. V.; Brinkmann, A.; Michaelis, V. K. Capturing Elusive Polymorphs of Curcumin: A Structural Characterization and Computational Study. *Crystal Growth and Design* **2018**, *18* (9), 5556–5563.
3. Emmler, T.; Gieschler, S.; Limbach, H. H.; Buntkowsky, G. A Simple Method for the Characterization of OHO-Hydrogen Bonds by ^{1}H-Solid State NMR Spectroscopy. *Journal of Molecular Structure* **2004**, *700* (1-3), 29–38.
4. Bell, R. A.; Chan, C. L.; Sayer, B. G. Deuterium Isotope Effects on ^{13}C Chemical Shifts in Benzene and Substituted Benzenes. *Journal of the Chemical Society, Chemical Communications* **1972**, No. 2, 67.
5. Lyssenko, K. A.; Lyubetsky, D. V.; Antipin, M. Y. Intramolecular H-Bonds in the Crystal of Tetraacetylethane: 3C-4E Interaction or a Dynamic Disorder? *Mendeleev Communications* **2003**, *13* (2), 60–62.
6. Piccoli, P. M.; Koetzle, T. F.; Schultz, A. J.; Zhurova, E. A.; Stare, J.; Pinkerton, A. A.; Eckert, J.; Hadzi, D. Variable Temperature Neutron Diffraction and X-Ray Charge Density Studies of Tetraacetylethane. *The Journal of Physical Chemistry A* **2008**, *112* (29), 6667–6677.
7. Altman, L. J.; Laungani, P.; Gunnarsson, G.; Wennerstrom, H.; Forsen, S. Proton, Deuterium, and Tritium Nuclear Magnetic Resonance of Intramolecular Hydrogen Bonds. Isotope Effects and the Shape of the Potential Energy Function. *Journal of the American Chemical Society* **1978**, *100* (26), 8264–8266.
8. Kagawa, H.; Sagawa, M.; Kakuta, A. 3-(4-Tert-Butylphenyl)-3-Hydroxy-1-(4-Methoxyphenyl)-2-Propen-1-One: An SHG Active β-Diketone. *Acta Crystallographica Section C Crystal Structure Communications* **1993**, *49* (12), 2181–2183.

9. Fulmer, G. R.; Miller, A. J.; Sherden, N. H.; Gottlieb, H. E.; Nudelman, A.; Stoltz, B. M.; Bercaw, J. E.; Goldberg, K. I. NMR Chemical Shifts of Trace Impurities: Common Laboratory Solvents, Organics, and Gases in Deuterated Solvents Relevant to the Organometallic Chemist. *Organometallics* **2010**, *29* (9), 2176–2179.
10. Arunan, E.; Desiraju, G. R.; Klein, R. A.; Sadlej, J.; Scheiner, S.; Alkorta, I.; Clary, D. C.; Crabtree, R. H.; Dannenberg, J. J.; Hobza, P.; Kjaergaard, H. G.; Legon, A. C.; Mennucci, B.; Nesbitt, D. J. Definition of the Hydrogen Bond (IUPAC Recommendations 2011). *Pure and Applied Chemistry* **2011**, *83* (8), 1637–1641.
11. Becker, E. D. Hydrogen Bonding. *Encyclopedia of Magnetic Resonance* **2007**.
12. Huggins, M. L. The Hydrogen Bond (Pimentel, George C.; McClellan, Aubrey L.). *Journal of Chemical Education* **1960**, *37* (11).
13. Steiner, T. The Hydrogen Bond in the Solid State. *Angewandte Chemie International Edition* **2002**, *41* (1), 48–76.
14. Jeffrey, J. G. A. *An Introduction to Hydrogen Bonding*; Oxford University Press: New York, 1997.
15. Maréchal Yves. *The Hydrogen Bond and the Water Molecule: The Physics and Chemistry of Water, Aqueous and Bio Media*; Elsevier: Amsterdam, 2007.
16. Emsley, J. Structure and Bonding. In *Complex chemistry*; Springer: Berlin, 1984; Vol. 57.
17. Hadži D. *Hydrogen Bonding: Papers Presented at the Symposium on Hydrogen Bonding*; Pergamon Press: London, 1959.
18. Zhou, J.; Lin, H.; Cheng, X.-F.; Shu, J.; He, J.-H.; Li, H.; Xu, Q.-F.; Li, N.-J.; Chen, D.-Y.; Lu, J.-M. Ultrasensitive and Robust Organic Gas Sensors through Dual Hydrogen Bonding. *Materials Horizons* **2019**, *6* (3), 554–562.
19. Jayaraman, A. 100th Anniversary of Macromolecular Science Viewpoint: Modeling and Simulation of Macromolecules with Hydrogen Bonds: Challenges, Successes, and Opportunities. *ACS Macro Letters* **2020**, *9* (5), 656–665.

20. Hutchins, K. M. Functional Materials Based on Molecules with Hydrogen-Bonding Ability: Applications to Drug Co-Crystals and Polymer Complexes. *Royal Society Open Science* **2018**, *5* (6), 180564.
21. Cao, J.; Lu, C.; Zhuang, J.; Liu, M.; Zhang, X.; Yu, Y.; Tao, Q. Multiple Hydrogen Bonding Enables the Self-Healing of Sensors for Human-Machine Interactions. *Angewandte Chemie International Edition* **2017**, *56* (30), 8795–8800.
22. Shokova, E. A.; Kim, J. K.; Kovalev, V. V. 1,3-Diketones. Synthesis and Properties. *Russian Journal of Organic Chemistry* **2015**, *51* (6), 755–830.
23. Pradhan, J.; Goyal, A. β-Diketones: Important Intermediates for Drug Synthesis. *International Journal of Pharmaceutical Research & Allied Sciences* **2015**, *4* (2), 1–18.
24. Kitos, A. A.; Mavragani, N.; Murugesu, M.; Brusso, J. L. A Chelate like No Other: Exploring the Synthesis, Coordination Chemistry and Applications of Imidoyl Amidine Frameworks. *Materials Advances* **2020**, *1* (8), 2688–2706.
25. Cowan, M. G.; Miller, R. G.; Southon, P. D.; Price, J. R.; Yazaydin, O.; Lane, J. R.; Kepert, C. J.; Brooker, S. Selective Gas Adsorption in a Pair of Robust Isostructural MOFs Differing in Framework Charge and Anion Loading. *Inorganic Chemistry* **2014**, *53* (22), 12076–12083.
26. Zebret, S.; Dupont, N.; Bernardinelli, G.; Hamacek, J. Self-Assembly of a Trinuclear Luminescent Europium Complex. *Chemistry - A European Journal* **2009**, *15* (14), 3355–3358.
27. Tautomerism https://www.britannica.com/science/tautomerism (accessed May 26, 2022).
28. Zielinski, T. J.; Grushow, A. Hydrogen Bonding Using NMR: A New Look at the 2,4-Pentanedione Keto-Enol Tautomer Experiment. *Journal of Chemical Education* **2002**, *79* (6), 707.
29. Boese, R.; Antipin, M. Y.; Bläser, D.; Lyssenko, K. A. Molecular Crystal Structure of Acetylacetone at 210 and 110 K: Is the Crystal Disorder Static or Dynamic? *The Journal of Physical Chemistry B* **1998**, *102* (44), 8654–8660.
30. Jeffrey, G. A.; Saenger, W. Hydrogen Bonding in Biological Structures. **1991**.

31. Gilli, P.; Bertolasi, V.; Ferretti, V.; Gilli, G. Evidence for Resonance-Assisted Hydrogen Bonding. 4. Covalent Nature of the Strong Homonuclear Hydrogen Bond. Study of the O-H--O System by Crystal Structure Correlation Methods. *Journal of the American Chemical Society* **1994**, *116* (3), 909–915.
32. Woińska, M.; Jayatilaka, D.; Spackman, M. A.; Edwards, A. J.; Dominiak, P. M.; Woźniak, K.; Nishibori, E.; Sugimoto, K.; Grabowsky, S. Hirshfeld Atom Refinement for Modelling Strong Hydrogen Bonds. *Acta Crystallographica Section A Foundations and Advances* **2014**, *70* (5), 483–498.
33. Malaspina, L. A.; Edwards, A. J.; Woińska, M.; Jayatilaka, D.; Turner, M. J.; Price, J. R.; Herbst-Irmer, R.; Sugimoto, K.; Nishibori, E.; Grabowsky, S. Predicting the Position of the Hydrogen Atom in the Short Intramolecular Hydrogen Bond of the Hydrogen Maleate Anion from Geometric Correlations. *Crystal Growth & Design* **2017**, *17* (7), 3812–3825.
34. Srinivasan, R.; Feenstra, J. S.; Park, S. T.; Xu, S.; Zewail, A. H. Direct Determination of Hydrogen-Bonded Structures in Resonant and Tautomeric Reactions Using Ultrafast Electron Diffraction. *Journal of the American Chemical Society* **2004**, *126* (8), 2266–2267.
35. Caminati, W.; Grabow, J.-U. The C_{2v} Structure of Enolic Acetylacetone. *Journal of the American Chemical Society* **2005**, *128* (3), 854–857.
36. Rocha, J.; Paz, F. A.; Sardo, M.; Mafra, L. Revisiting the Crystal Structure of Dickite: X-Ray Diffraction, Solid-State NMR, and DFT Calculations Study. *American Mineralogist* **2018**, *103* (5), 812–818.
37. Clark, S. J.; Segall, M. D.; Pickard, C. J.; Hasnip, P. J.; Probert, M. I.; Refson, K.; Payne, M. C. First Principles Methods Using CASTEP. *Zeitschrift für Kristallographie - Crystalline Materials* **2005**, *220* (5-6), 567–570.
38. Dannenberg, J. J.; Rios, R. Theoretical Study of the Enolic Forms of Acetylacetone. How Strong Is the Hydrogen Bond? *The Journal of Physical Chemistry* **1994**, *98* (27), 6714–6718.
39. Broadbent, S. A.; Burns, L. A.; Chatterjee, C.; Vaccaro, P. H. Investigation of Electronic Structure and Proton Transfer in Ground State Acetylacetone. *Chemical Physics Letters* **2007**, *434* (1-3), 31–37.

40. Kong, X.; Brinkmann, A.; Terskikh, V.; Wasylishen, R. E.; Bernard, G. M.; Duan, Z.; Wu, Q.; Wu, G. Proton Probability Distribution in the O···H···O Low-Barrier Hydrogen Bond: A Combined Solid-State NMR and Quantum Chemical Computational Study of Dibenzoylmethane and Curcumin. *The Journal of Physical Chemistry B* **2016**, *120* (45), 11692–11704.
41. Hansen, P. Isotope Effects on Chemical Shifts in the Study of Intramolecular Hydrogen Bonds. *Molecules* **2015**, *20* (2), 2405–2424.
42. McDermott, A.; Ridenour, C. F. Proton Chemical Shift Measurements in Biological Solids. *Encyclopedia of Magnetic Resonance* **2007**.
43. Mildvan, A. S.; Harris, T. K.; Abeygunawardana, C. Nuclear Magnetic Resonance Methods for the Detection and Study of Low-Barrier Hydrogen Bonds on Enzymes. *Methods in Enzymology* **1999**, 219–245.
44. Harris, T. K.; Mildvan, A. S. High-Precision Measurement of Hydrogen Bond Lengths in Proteins by Nuclear Magnetic Resonance Methods. *Proteins: Structure, Function, and Genetics* **1999**, *35* (3), 275–282.
45. Brunner, E.; Sternberg, U. Solid-State NMR Investigations on the Nature of Hydrogen Bonds. *Progress in Nuclear Magnetic Resonance Spectroscopy* **1998**, *32* (1), 21–57.
46. Shenderovich, I. G.; Tolstoy, P. M.; Golubev, N. S.; Smirnov, S. N.; Denisov, G. S.; Limbach, H.-H. Low-Temperature NMR Studies of the Structure and Dynamics of a Novel Series of Acid−Base Complexes of HF with Collidine Exhibiting Scalar Couplings across Hydrogen Bonds. *Journal of the American Chemical Society* **2003**, *125* (38), 11710–11720.
47. Smirnov, S. N.; Benedict, H.; Golubev, N. S.; Denisov, G. S.; Kreevoy, M. M.; Schowen, R. L.; Limbach, H.-H. Exploring Zero-Point Energies and Hydrogen Bond Geometries along Proton Transfer Pathways by Low-Temperature NMR. *Canadian Journal of Chemistry* **1999**, *77* (5-6), 943–949.
48. Lorente, P.; Shenderovich, I. G.; Golubev, N. S.; Denisov, G. S.; Buntkowsky, G.; Limbach, H.-H. $^{1}H/^{15}N$ NMR Chemical Shielding, Dipolar $^{15}N,^{2}H$ Coupling and Hydrogen Bond Geometry Correlations in a Novel Series of Hydrogen-

Bonded Acid-Base Complexes of Collidine with Carboxylic Acids. *Magnetic Resonance in Chemistry* **2001**, *39* (S1).

49. Benedict, H.; Limbach, H.-H.; Wehlan, M.; Fehlhammer, W.-P.; Golubev, N. S.; Janoschek, R. Solid State ^{15}N NMR and Theoretical Studies of Primary and Secondary Geometric H/D Isotope Effects on Low-Barrier NHN−Hydrogen Bonds. *Journal of the American Chemical Society* **1998**, *120* (12), 2939–2950.
50. Hansen, P. E. Deuterium Isotope Effects on the ^{13}C Nuclear Shielding of Intramolecularly Hydrogen-Bonded Systems. *Magnetic Resonance in Chemistry* **1986**, *24* (10), 903–910.
51. Bolvig, S.; Hansen, P. E.; Morimoto, H.; Wemmer, D.; Williams, P. Primary Tritium and Deuterium Isotope Effects on Chemical Shifts of Compounds Having an Intramolecular Hydrogen Bond. *Magnetic Resonance in Chemistry* **2000**, *38* (7), 525–535.
52. Bolvig, S.; Erik Hansen, P. Isotope Effects on Chemical Shifts as an Analytical Tool in Structural Studies of Intramolecular Hydrogen Bonded Compounds. *Current Organic Chemistry* **2000**, *4* (1), 19–54.
53. Jameson, C. J.; Osten, H. J. Theoretical Aspects of Isotope Effects on Nuclear Shielding. *Annual Reports on NMR Spectroscopy* **1986**, 1–78.
54. Reuben, J. Intramolecular Hydrogen Bonding as Reflected in the Deuterium Isotope Effects on Carbon-13 Chemical Shifts. Correlation with Hydrogen Bond Energies. *Journal of the American Chemical Society* **1986**, *108* (8), 1735–1738.
55. Hansen, P. E. Hydrogen Bonding and Tautomerism Studied by Isotope Effects on Chemical Shifts. *Journal of Molecular Structure* **1994**, *321* (1-2), 79–87.
56. Bolvig, S.; Hansen, P. E. Deuterium-Induced Isotope Effects on ^{13}C Chemical Shifts as a Probe for Tautomerism in Enolic β-Diketones. *Magnetic Resonance in Chemistry* **1996**, *34* (6), 467–478.
57. Perrin, C. L. Symmetry of Hydrogen Bonds in Solution. *Pure and Applied Chemistry* **2009**, *81* (4), 571–583.
58. Schaefer, J. P.; Wheatley, P. J. The Crystal and Molecular Structure of Tetra-Acetylethane. *Journal of the Chemical Society A: Inorganic, Physical, Theoretical* **1966**, 528.

59. Zhang, Y.; Wang, S.; Enright, G. D.; Breeze, S. R. Tetraacetylethane Dianion (TAE) as a Bridging Ligand for Molecular Square Complexes: $Co^{II}_4(Tae)_4(Dpa)_4$, DPA = Di-2-Pyridylamine, a Chiral Molecular Square in the Solid State. *Journal of the American Chemical Society* **1998**, *120* (36), 9398–9399.
60. Guermoune, A.; Hilke, M. Fullerenic Particles for the Growth of Carbon Nanowall-like Flowers on Multilayer Graphene. *Nanotechnology* **2016**, *27* (17), 175603.
61. Power, L. F.; Turner, K. E.; Moore, F. H. Refinement of the Crystal and Molecular Structure of Tetraacetylethane by Neutron Diffraction. *Journal of Crystal and Molecular Structure* **1975**, *5* (1), 59–66.
62. Kearley, G. J.; Stare, J.; Kutteh, R.; Daemen, L. L.; Hartl, M. A.; Eckert, J. Methyl Dynamics Flattens Barrier to Proton Transfer in Crystalline Tetraacetylethane. *The Journal of Physical Chemistry A* **2012**, *116* (9), 2283–2291.
63. Takegoshi, K.; McDowell, C. A. ^{13}C Chemical Shielding Tensors in Single Crystals of Tetraacetylethane. *Chemical Physics Letters* **1986**, *123* (3), 159–163.
64. Emsley, J.; Ma, L. Y.; Bates, P. A.; Motevalli, M.; Hursthouse, M. B. Cheminform Abstract: β-Diketone Interactions. Part 8. the Hydrogen Bonding of the Enol Tautomers of Some 3-Substituted Pentane-2,4-Diones. *ChemInform* **1989**, *20* (37).
65. Spencer, J. N.; Holmboe, E. S.; Kirshenbaum, M. R.; Firth, D. W.; Pinto, P. B. Solvent Effects on the Tautomeric Equilibrium of 2,4-Pentanedione. *Canadian Journal of Chemistry* **1982**, *60* (10), 1178–1182.
66. Powling, J.; Bernstein, H. J. The Effect of Solvents on Tautomeric Equilibria. *Journal of the American Chemical Society* **1951**, *73* (9), 4353–4356.
67. Spectral database for organic compounds, SDBS https://sdbs.db.aist.go.jp/sdbs/cgi-bin/direct_frame_top.cgi (accessed May 27, 2022).
68. Bernard, G. M.; Goyal, A.; Miskolzie, M.; McKay, R.; Wu, Q.; Wasylishen, R. E.; Michaelis, V. K. Methylammonium Lead Chloride: A Sensitive Sample for

an Accurate NMR Thermometer. *Journal of Magnetic Resonance* **2017**, *283*, 14–21.

69. Somorjai, R. L.; Hornig, D. F. Double-Minimum Potentials in Hydrogen-Bonded Solids. *The Journal of Chemical Physics* **1962**, *36* (8), 1980–1987.
70. O'Leary, D. J.; Hickstein, D. D.; Hansen, B. K.; Hansen, P. E. Theoretical and NMR Studies of Deuterium Isotopic Perturbation of Hydrogen Bonding in Symmetrical Dihydroxy Compounds. *The Journal of Organic Chemistry* **2009**, *75* (5), 1331–1342.
71. Matta, M. K.; Florian, J.; Zusterzeel, R.; Pilli, N. R.; Patel, V.; Volpe, D. A.; Yang, Y.; Oh, L.; Bashaw, E.; Zineh, I.; Sanabria, C.; Kemp, S.; Godfrey, A.; Adah, S.; Coelho, S.; Wang, J.; Furlong, L.-A.; Ganley, C.; Michele, T.; Strauss, D. G. Effect of Sunscreen Application on Plasma Concentration of Sunscreen Active Ingredients. *JAMA* **2020**, *323* (3), 256.
72. Stien, D.; Clergeaud, F.; Rodrigues, A. M.; Lebaron, K.; Pillot, R.; Romans, P.; Fagervold, S.; Lebaron, P. Metabolomics Reveal That Octocrylene Accumulates in *Pocillopora Damicornis* Tissues as Fatty Acid Conjugates and Triggers Coral Cell Mitochondrial Dysfunction. *Analytical Chemistry* **2018**, *91* (1), 990–995.
73. Kockler, J.; Robertson, S.; Oelgemöller, M.; Davies, M.; Bowden, B.; Brittain, H. G.; Glass, B. D. Butyl Methoxy Dibenzoylmethane. *Profiles of Drug Substances, Excipients and Related Methodology* **2013**, 87–111.
74. Murphy, R. B.; Staton, J.; Rawal, A.; Darwish, T. A. The Effect of Deuteration on the Keto–Enol Equilibrium and Photostability of the Sunscreen Agent Avobenzone. *Photochemical & Photobiological Sciences* **2020**, *19* (10), 1410–1422.
75. Ferreira, P. J. O.; Pinto da Silva, L.; Duarte, D. J. R.; Miranda, M. S.; Esteves da Silva, J. C. G. A Computational Study of the Structure, Aromaticity and Enthalpy of Formation of UVA Filter 4-Tert-Butyl-4′-Methoxydibenzoylmethane. *Computational and Theoretical Chemistry* **2014**, *1038*, 6–16.
76. Pinto da Silva, L.; Ferreira, P. J.; Duarte, D. J.; Miranda, M. S.; Esteves da Silva, J. C. Structural, Energetic, and UV–Vis Spectral Analysis of UVA Filter 4-*Tert*-

Butyl-4′-Methoxydibenzoylmethane. *The Journal of Physical Chemistry A* **2014**, *118* (8), 1511–1518.

77. Bordi, F.; Cametti, C. Biomembranes. *Encyclopedia of Condensed Matter Physics* **2005**, 116–122.
78. Scott, A. F.; Luk, L. Y. P.; Allemann, R. K. Chemical Ligation and Isotope Labeling to Locate Dynamic Effects. *Measurement and Analysis of Kinetic Isotope Effects* **2017**, 23–41.
79. Zoi, I.; Antoniou, D.; Schwartz, S. D. Linking Protein Dynamics to Enzyme Catalysis. *Comprehensive Natural Products III* **2020**, 578–588.
80. Kempf, J. G.; Loria, J. P. Protein Dynamics from Solution NMR. *Cell Biochemistry and Biophysics* **2002**, *37* (3), 187–212.
81. Kovermann, M.; Rogne, P.; Wolf-Watz, M. Protein Dynamics and Function from Solution State NMR Spectroscopy. *Quarterly Reviews of Biophysics* **2016**, *49*.
82. Opella, S. J.; Marassi, F. M. Applications of NMR to Membrane Proteins. *Archives of Biochemistry and Biophysics* **2017**, *628*, 92–101.
83. Akbey, Ü.; Oschkinat, H. Structural Biology Applications of Solid-State MAS DNP NMR. *Journal of Magnetic Resonance* **2016**, *269*, 213–224.
84. van der Wel, P. C. A. New Applications of Solid-State NMR in Structural Biology. *Emerging Topics in Life Sciences* **2018**, *2* (1), 57–67.
85. Cheng, X.; Jo, S.; Qi, Y.; Marassi, F. M.; Im, W. Solid-State NMR-Restrained Ensemble Dynamics of a Membrane Protein in Explicit Membranes. *Biophysical Journal* **2015**, *108* (8), 1954–1962.
86. Mandala, V. S.; Williams, J. K.; Hong, M. Structure and Dynamics of Membrane Proteins from Solid-State NMR. *Annual Review of Biophysics* **2018**, *47* (1), 201–222.
87. Li, W.; Mcdermott, A. E. Detection of Slow Dynamics by Solid-State NMR: Application to L-Phenylalanine Hydrochloride. *Concepts in Magnetic Resonance Part A* **2013**, *42A* (1), 14–22.
88. Mizuno, M.; Chizuwa, M.; Umiyama, T.; Kumagai, Y.; Miyatou, T.; Ohashi, R.; Ida, T.; Tansho, M.; Shimizu, T. Local Structure and Molecular Motions in

Imidazolium Hydrogen Malonate Crystal as Studied by ^{2}H and ^{13}C NMR. *Hyperfine Interactions* **2015**, *230* (1-3), 95–100.

89. Facelli, J. C.; Orendt, A. M.; Jiang, Y. J.; Pugmire, R. J.; Grant, D. M. Carbon-13 Chemical Shift Tensors and Molecular Conformation of Anisole. *The Journal of Physical Chemistry* **1996**, *100* (20), 8268–8272.
90. Penner, G. H.; Wasylishen, R. E. A Carbon-13 CP/MAS Nuclear Magnetic Resonance Study of Several 1,4-Disubstituted Benzenes in the Solid State. *Canadian Journal of Chemistry* **1989**, *67* (3), 525–534.
91. Harris, R. K. Chemical Exchange and Quadrupolar Effects. In *Nuclear magnetic resonance spectroscopy: A physicochemical view*; Longman Scientific & Technical: Burnt Mill, Harlow, Essex, England, 1997; pp 122–127.
92. Casarini, D.; Lunazzi, L.; Mazzanti, A. Cheminform Abstract: Recent Advances in Stereodynamics and Conformational Analysis by Dynamic NMR and Theoretical Calculations. *ChemInform* **2010**, *41* (29).
93. Wasylishen, R. E. Ring Inversion in Solid Fluorocyclohexane. *Canadian Journal of Chemistry* **1986**, *64* (10), 2094–2095.
94. Cortés-Guzmán, F.; Cuevas, G.; Martín Pendás, Á.; Hernández-Trujillo, J. The Rotational Barrier of Ethane and Some of Its Hexasubstituted Derivatives in Terms of the Forces Acting on the Electron Distribution. *Physical Chemistry Chemical Physics* **2015**, *17* (29), 19021–19029.
95. Drakenberg, T.; Forsen, S. Barrier to Internal Rotation of Amides. I. Formamide. *The Journal of Physical Chemistry* **1970**, *74* (1), 1–7.
96. Lukin, S.; Stolar, T.; Tireli, M.; Blanco, M. V.; Babić, D.; Friščić, T.; Užarević, K.; Halasz, I. Tandem in Situ Monitoring for Quantitative Assessment of Mechanochemical Reactions Involving Structurally Unknown Phases. *Chemistry - A European Journal* **2017**, *23* (56), 13941–13949.
97. Lukin, S.; Tireli, M.; Stolar, T.; Barišić, D.; Blanco, M. V.; di Michiel, M.; Užarević, K.; Halasz, I. Isotope Labeling Reveals Fast Atomic and Molecular Exchange in Mechanochemical Milling Reactions. *Journal of the American Chemical Society* **2019**, *141* (3), 1212–1216.

98. Métro, T.-X.; Gervais, C.; Martinez, A.; Bonhomme, C.; Laurencin, D. Unleashing the Potential of ^{17}O NMR Spectroscopy Using Mechanochemistry. *Angewandte Chemie* **2017**, *129* (24), 6907–6911.
99. Claridge, T. D. *High-Resolution NMR Techniques in Organic Chemistry*; Elsevier: Amsterdam, 2016.
100. Levitt, M. H. *Spin Dynamics: Basics of Nuclear Magnetic Resonance*; Wiley: Chichester, 2015.
101. Rahman, A.-U.; Choudhary, M. I.; Wahab, A.-tul. *Solving Problems with NMR Spectroscopy*; Academic Press: Amsterdam, 2016.
102. Kalinowski, H.-O.; Becconsall, J. K.; Kalinowski, H.-O. *Carbon-13 NMR Spectroscopy*; Wiley: Chichester, 1988.
103. Silverstein, R. M.; Webster, F. X.; Kiemle, D. J.; Bryce, D. L. *Spectrometric Identification of Organic Compounds*; Wiley: Hoboken, N.J, 2015.
104. Perdew, J. P.; Burke, K.; Ernzerhof, M. Generalized Gradient Approximation Made Simple. *Physical Review Letters* **1996**, *77* (18), 3865–3868.
105. Pickard, C. J.; Mauri, F. All-Electron Magnetic Response with Pseudopotentials: NMR Chemical Shifts. *Physical Review B* **2001**, *63* (24).
106. Yates, J. R.; Pickard, C. J.; Mauri, F. Calculation of NMR Chemical Shifts for Extended Systems Using Ultrasoft Pseudopotentials. *Physical Review B* **2007**, *76* (2).

APPENDIX A
Avobenzone Solution NMR Spectra

Experimental Methods

The solution spectra were acquired on Agilent/Varian Inova three-channel 400 MHz spectrometer. The approximate concentration of avobenzone in $CDCl_3$ was 270 mM and the spectra were acquired at 26.9 °C, referenced to $CDCl_3$ at 77.06 ppm for ^{13}C and at 7.26 ppm for ^{1}H.

Introduction

This appendix includes a selection of 1- and 2-D ^{13}C and ^{1}H solution NMR spectra of avobenzone that allowed to confirm and clarify peak assignments already available in the literature.[73]

Our peak assignments are in perfect agreement with this of Kockler et al.[73] however the authors provided only 1-D ^{1}H and ^{13}C solution spectra. To verify peak assignments, we repeated 1-D NMR experiments and completed a series of 2-D experiments on natural abundance and deuterium labelled avobenzone. Clarification provided by the APT, gCOSY, ROESY, gHSQCAD and gHMBCAD was necessary to confirm the assignments, that, in turn was crucial to better understand and interpret NMR spectra of avobenzone in the solid state.[99–101]

APPENDIX A
Avobenzone Solution NMR Spectra

1. One-dimensional ^{13}C solution NMR

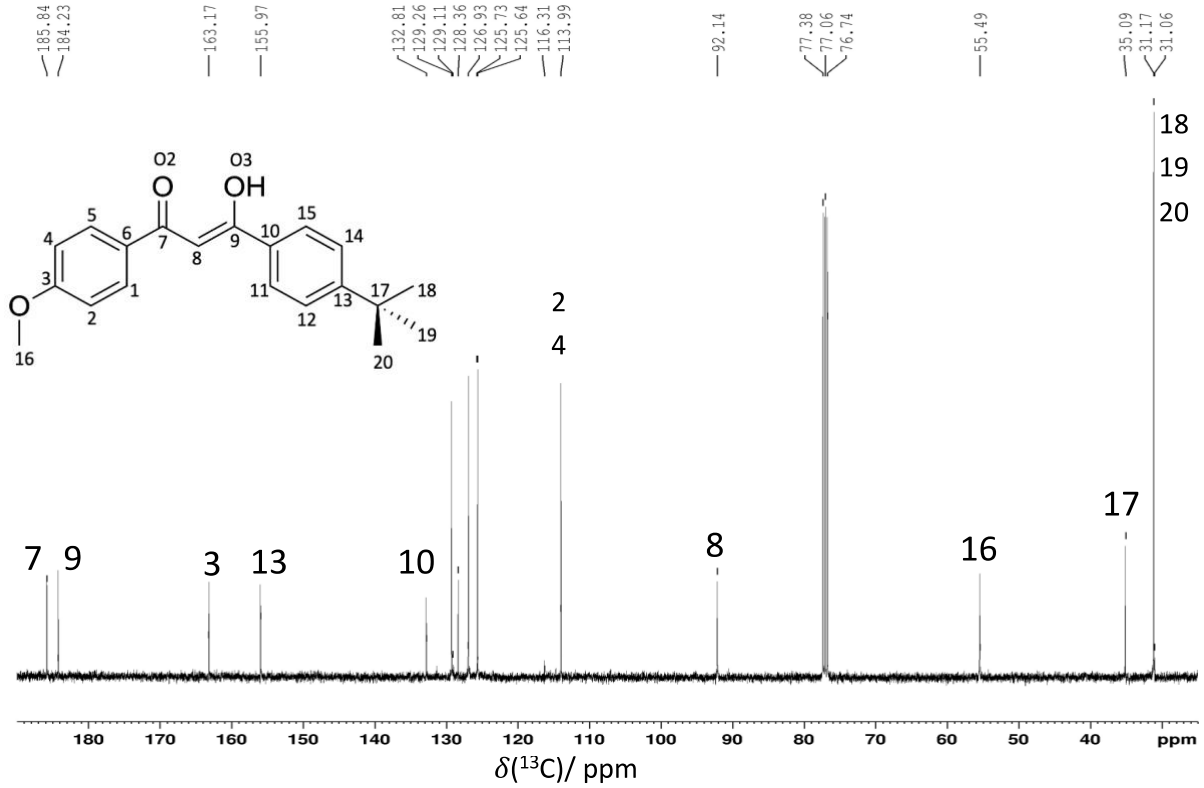

Figure 1A. C-13 NMR spectrum of approximately 270 mM solution of avobenzone in $CDCl_3$ acquired at 400 MHz and 26.9 °C, referenced to $CDCl_3$ at 77.06 ppm. The assignment of peaks in the 125.64-132.81 ppm range is provided in the next sections.

To assign the carbon peaks presented in Fig. 1A, the following experiments have been performed.

2. Attached Proton Test (APT)

Attached Proton Test (APT) is an example of one-dimensional ^{13}C NMR experiment that allows one to distinguish between quaternary (C) and methylene (CH_2) peaks from methine (CH) and methyl (CH_3) ^{13}C NMR peaks. It is an example of a spin-echo experiment (using two successive radiofrequency pulses to refocus spin magnetization). APT uses $^1J_{CH}$ interaction to change sign of signals, yielding positive CH and CH_3 and negative C and CH_2 peaks.

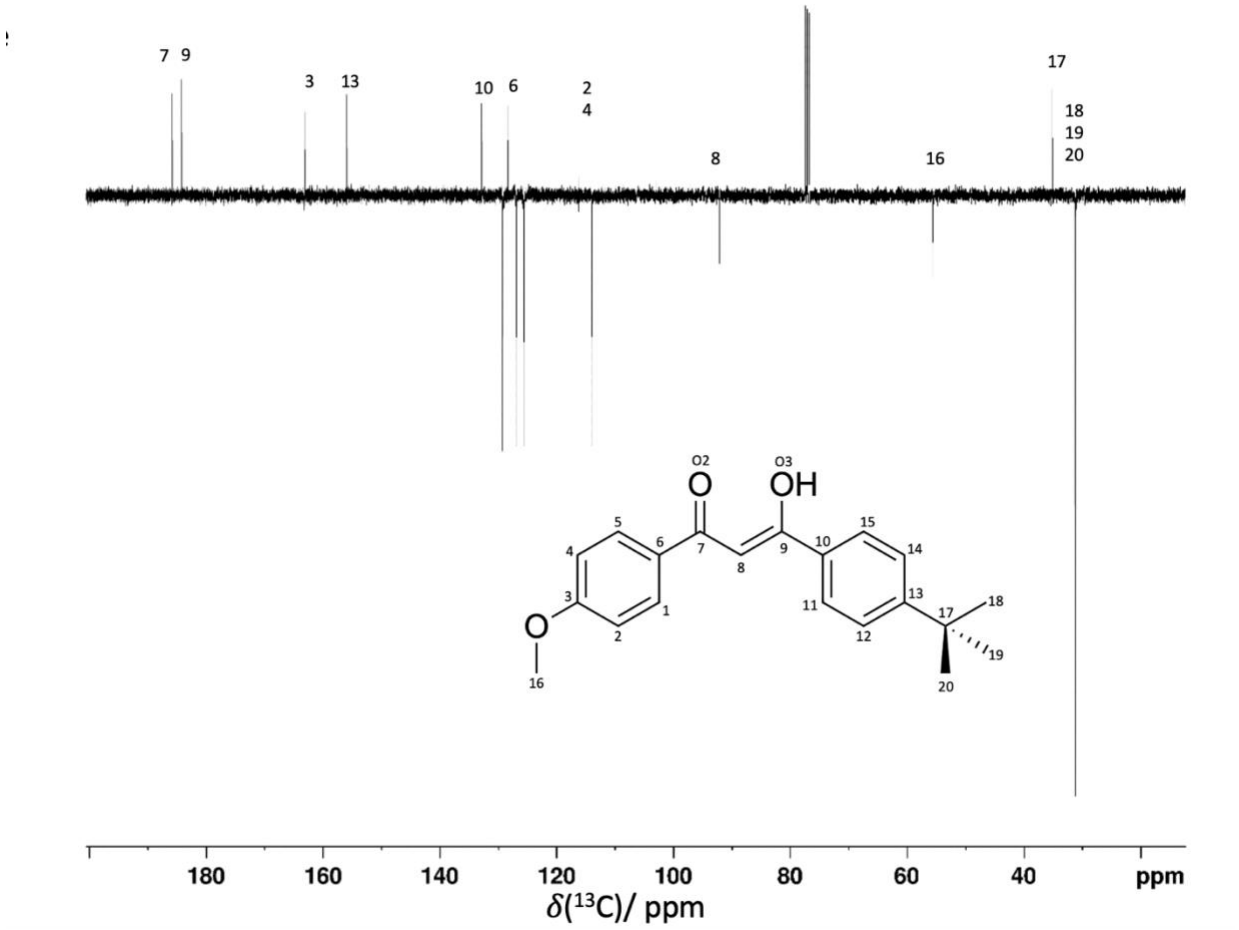

Figure 2A. Attached Proton Test (APT) ^{13}C spectrum of avobenzone. Methine and methyl (CH and CH_3) signals have negative phase, quaternary, and methylene (C and CH_2) carbons have positive phase.

In case of the avobenzone molecule, there are only two CH_3 groups: one in the methoxy part of the molecule and three in the *tert*-butyl part. Their assignment in APT is straightforward, as the most deshielded and intense signal of negative phase has a chemical shift of approximately 31 ppm, typical for methyl groups. The next negative, more deshielded peak at approximately 56 ppm is assigned as methoxy group, falling in the typical chemical shift range reported for -OCH_3.[102,103]

Having eliminated the CH_3 carbon signals, the rest of negative peaks arise due to CH carbons. This includes C8, assigned at approximately 92 ppm and aromatic carbons. From the APT spectrum alone, it was possible to distinguish aromatic carbons adjacent to the methoxy group (C2 and C4) at 114 ppm. The assignment of the remaining peaks in the aromatic region 125-133 ppm required additional experiments.

3. ^{1}H Solution NMR

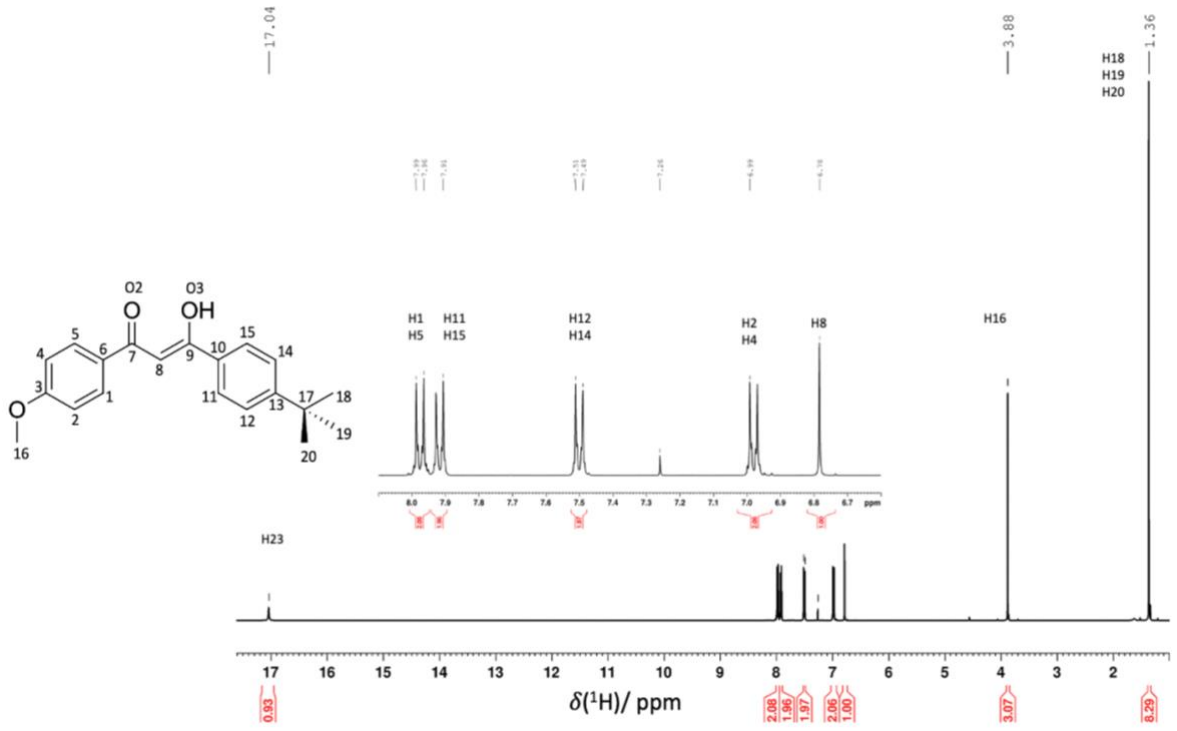

Figure 3A. H-1 NMR spectrum of avobenzone with aromatic region enlarged (inset). Hydrogen atom numbering is the same as for the carbon atoms; enolic proton is labeled as H23.

The ^{1}H NMR peak assignment was significantly facilitated with peak integration. Having set H8 integration to one atom, the rest of the peak assignments are consistent with what would be expected for avobenzone molecule. The most shielded peak at 1.36 ppm integrated to nine atoms corresponds to three methyl groups on the *tert*-butyl substituent. The more shielded singlet at 3.9 ppm corresponds to three hydrogen atoms on the methoxy group (H16). The most deshielded peak at 17 ppm arises from enolic proton H23, in the range previously reported in the literature.[103]

The preliminary assignment of the aromatic region was possible by the analysis of peak multiplicity and integration but did not allow to distinguish between specific hydrogen atoms (i.e., it was impossible to unequivocally determine whether the doublet at 7 ppm was due to H2,4 or H12,14 pairs).

4. Correlation Spectroscopy (COSY)

Correlation Spectroscopy (COSY) is a two-dimensional NMR technique that allows to determine *J*-coupling between ^{1}H-^{1}H nuclei (homonuclear) or between ^{1}H-^{13}C nuclei (heteronuclear). Both axes of the spectrum describe chemical shifts of the coupled nuclei, with cross-peaks indicating which nuclei are coupled to which other nuclei.[101]

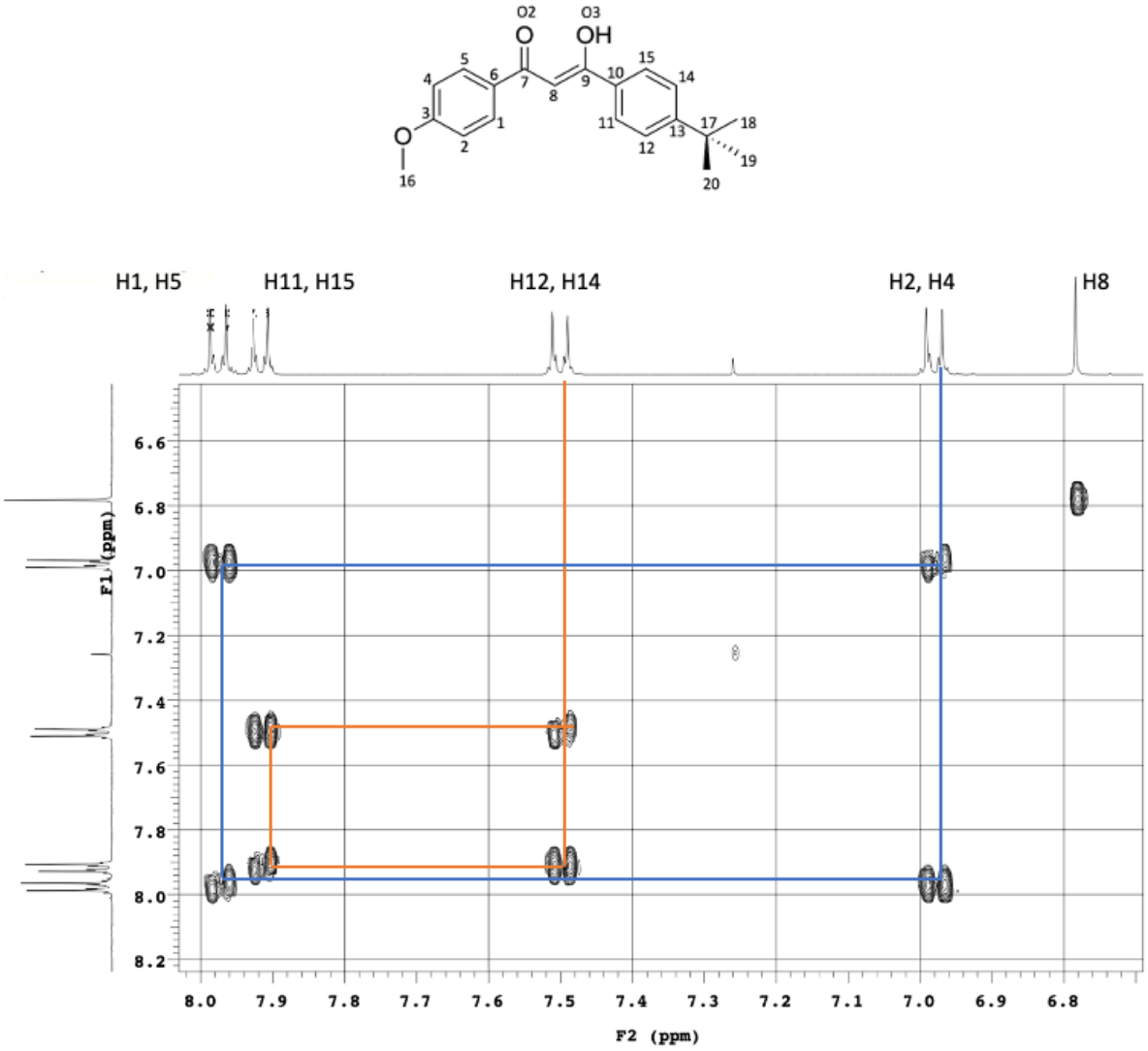

Figure 4A. Gradient correlation spectroscopy (gCOSY) spectrum of avobenzone in $CDCl_3$. Cross-peaks appear between protons that have a three-bond spin-spin coupling $^3J_{HH}$.

5. Rotating Frame Overhauser Effect Spectroscopy (ROESY)

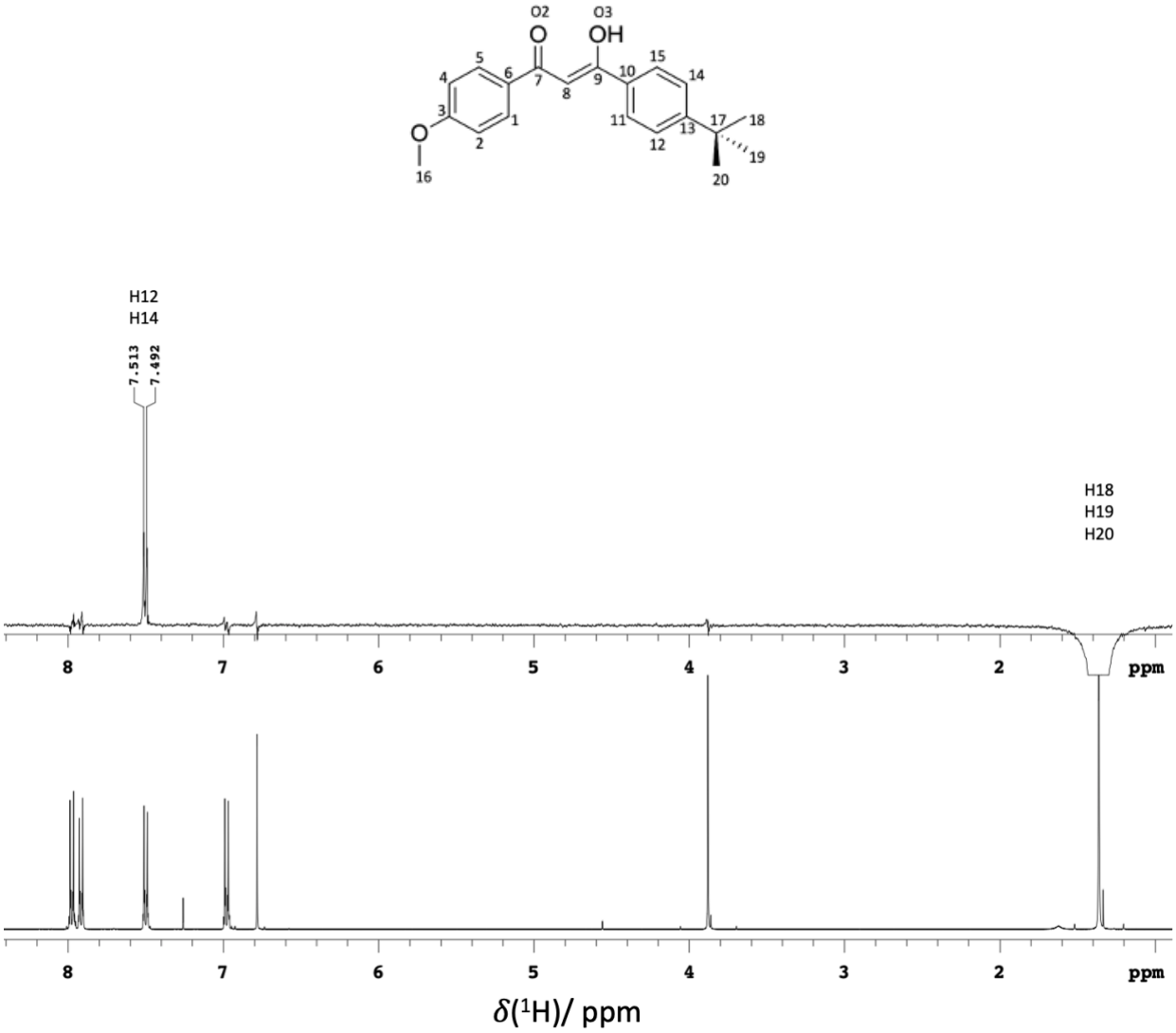

Figure 5A. ^{1}H Rotating frame Overhauser effect spectroscopy (ROESY) NMR spectrum of avobenzone (top) in comparison with ^{1}H spectrum (bottom).

Rotating Overhauser Effect (ROE) arises from protons with direct dipolar interactions. Since the inverted peak at 1.36 ppm is due to *tert*-butyl group, the peaks at 7.51 ppm and 7.49 ppm are the aromatic protons H12 and H14, adjacent to the *tert*-butyl group.

6. Gradient selected Heteronuclear Single Quantum Correlation (gHSQCAD)

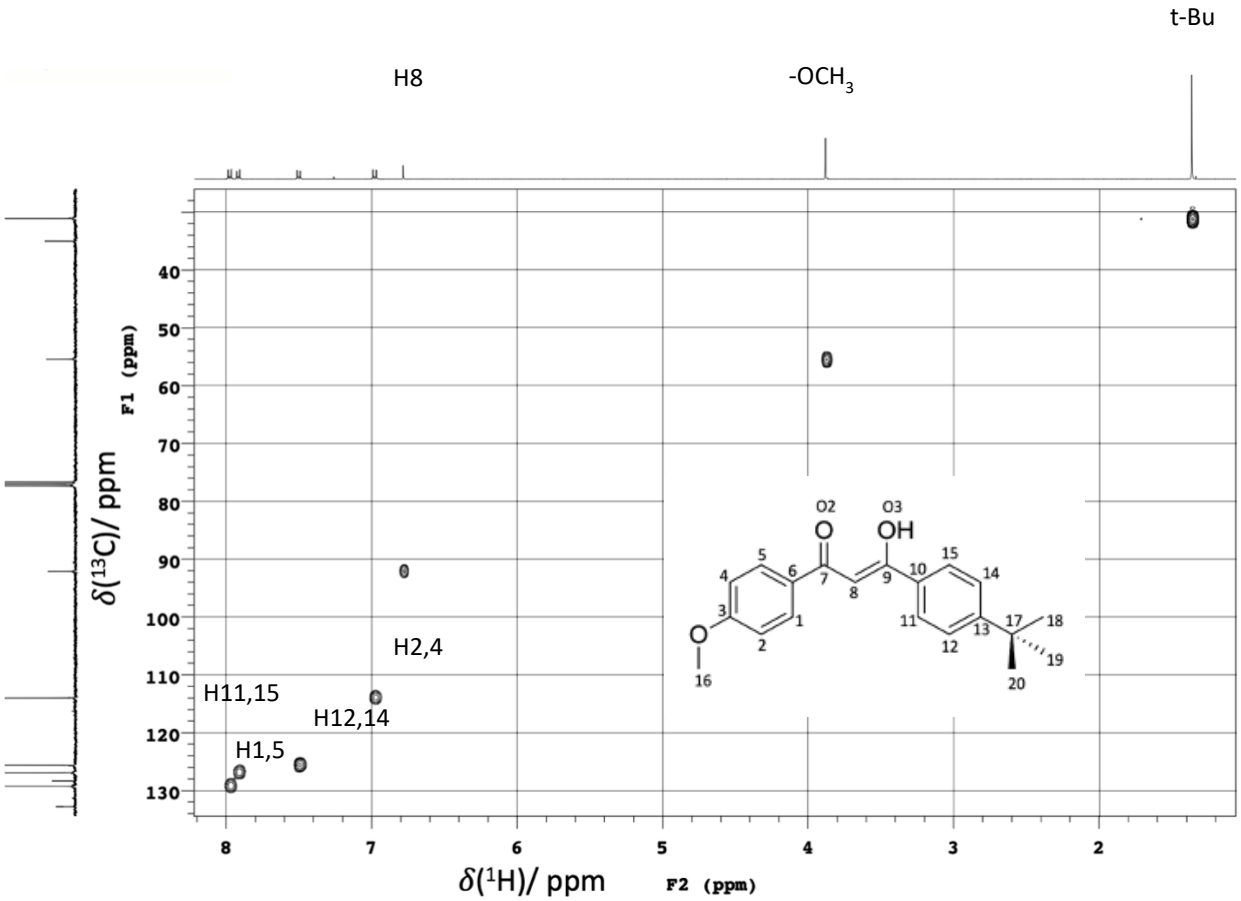

Figure 6A. ^{1}H-^{13}C Gradient selected Heteronuclear Single Quantum Correlation (gHSQCAD) spectrum of avobenzone.

Cross-peaks in Fig. 22 indicate hydrogen atoms (horizontal axis) directly attached to corresponding carbon atoms (vertical axis). Therefore, C3, C6, C7, C9, C10, C13 and C17 do not have cross-peaks, as they are not directly attached to any hydrogen atoms.

7. C-13 and ^{1}H solution spectra of deuterium labelled avobenzone (avobenzone-OD).

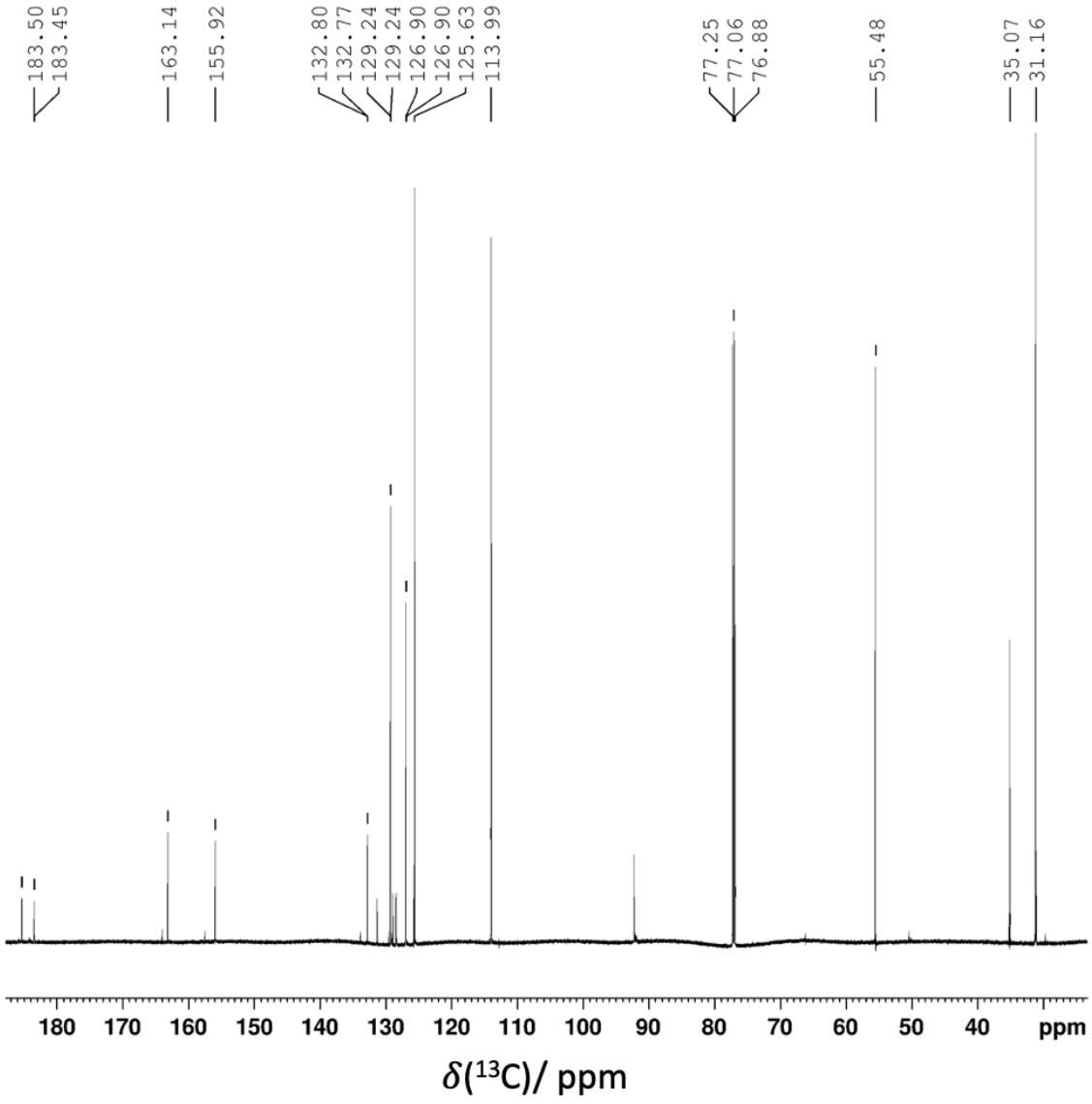

Figure 7A. C-13 NMR spectrum of approximately 270 mM solution of avobenzone-OD in $CDCl_3$ acquired at 700 MHz and 27.0 °C, referenced to $CDCl_3$ at 77.06 ppm.

APPENDIX A
Avobenzone Solution NMR Spectra

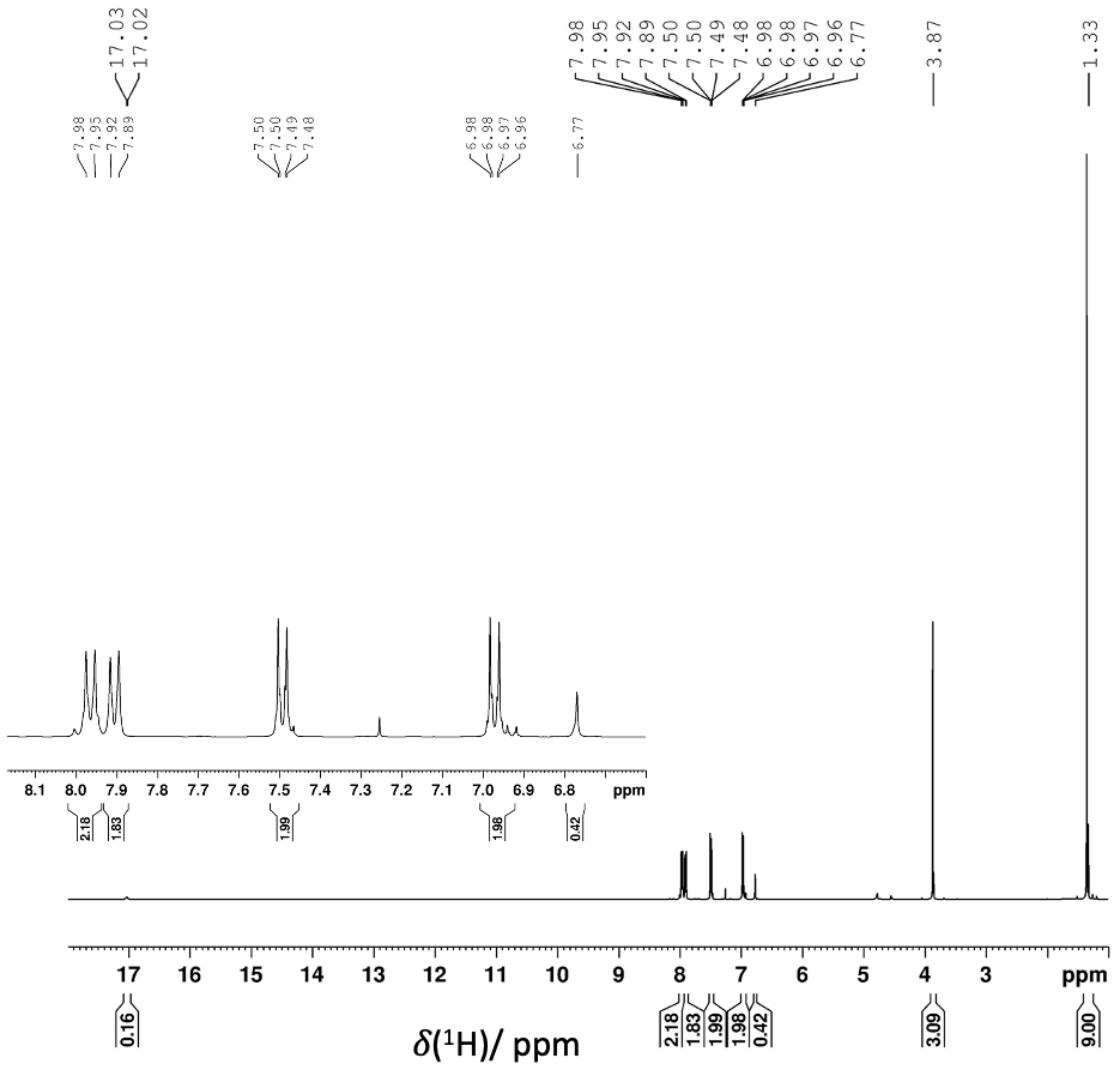

Figure 8A. H-1 NMR spectrum of approximately 270 mM solution of avobenzone-OD in $CDCl_3$ acquired at 700 MHz and 27.0 °C, referenced to $CDCl_3$ at 7.26 ppm.

APPENDIX A
Avobenzone Solution NMR Spectra

Table 1A. Summary of solution ^{1}H and ^{13}C NMR peak assignments of avobenzone.

Atom	$\delta(^{1}H)$/ ppm ± 0.01 ppm Natural abundance	$\delta(^{1}H)$/ ppm ± 0.01 ppm Avobenzone-OD
t-Bu	1.36	1.33
OCH_3	3.88	3.87
H8	6.78	6.77
H2, H4	6.98	6.98
H12, H14	7.50	7.50
H11, H15	7.92	7.91
H1, H5	7.98	7.97
OH	17.04	17.03
Atom	$\delta(^{13}C)$/ ppm ± 0.01 ppm	$\delta(^{13}C)$/ ppm ± 0.01 ppm
$-(CH_3)_3$	31.17	31.16
C13	35.09	35.07
C16	55.50	55.48
C8	92.14	92.21
C2, C4	113.99	113.99
C12, C14	125.64	125.63
C11, C15	126.93	126.90
C6	128.36	128.45
C1, C5	129.26	129.24
C10	132.81	132.79
C13	155.97	155.92
C3	163.17	163.14
C9	184.24	183.45
C7	185.84	183.50

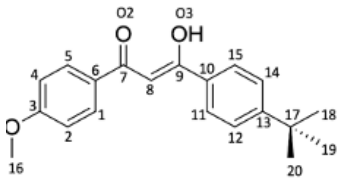

APPENDIX B
Tetraacetylethane Solution NMR Spectra

Experimental Methods

The ^{13}C solution spectra were acquired on Agilent/Varian VNMRS two-channel 500 MHz spectrometer with C13/H1 dual cold probe. The approximate concentration of TAE in $CDCl_3$ was 210 mM and the spectra were acquired at 27.0 °C, referenced to $CDCl_3$ at 77.06 ppm. The solution ^{1}H solution spectra were acquired on Agilent/Varian Inova three-channel 400 MHz spectrometer at 26.9 °C, referenced to $CDCl_3$ at 7.26 ppm.

1. One-dimensional ^{13}C solution NMR

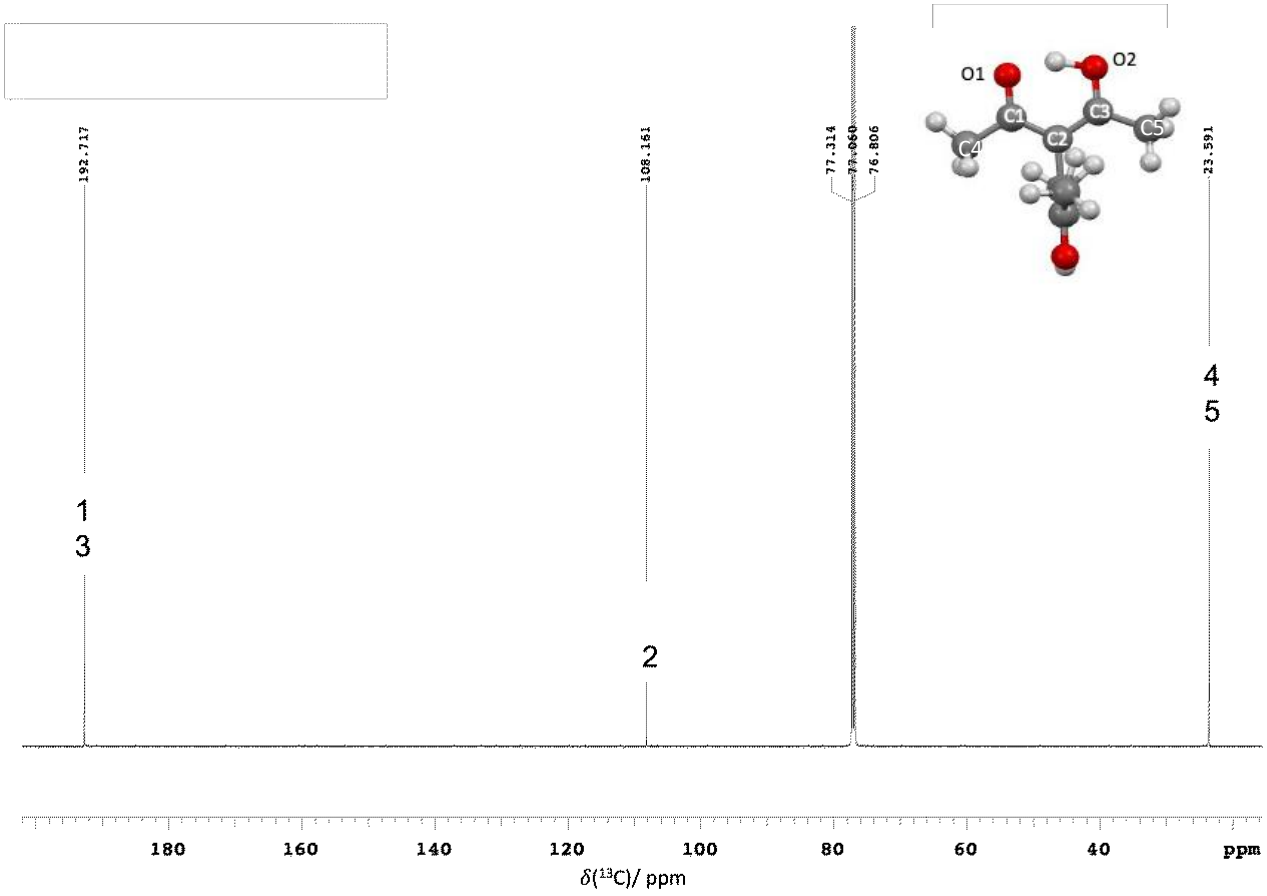

Figure 1B. C-13 NMR spectrum of approximately 210 mM solution of TAE in $CDCl_3$ acquired at 500 MHz and 27.0 °C, referenced to $CDCl_3$ at 77.06 ppm.

APPENDIX B
Tetraacetylethane Solution NMR Spectra

In contrast to the TAE in the solid state, the carbon nuclei C1/C3 and methyl C4/C5 are indistinguishable due to the rapid molecular motion in solution and the spectrum resembles this of acetylacetone.

2. ^{1}H Solution NMR

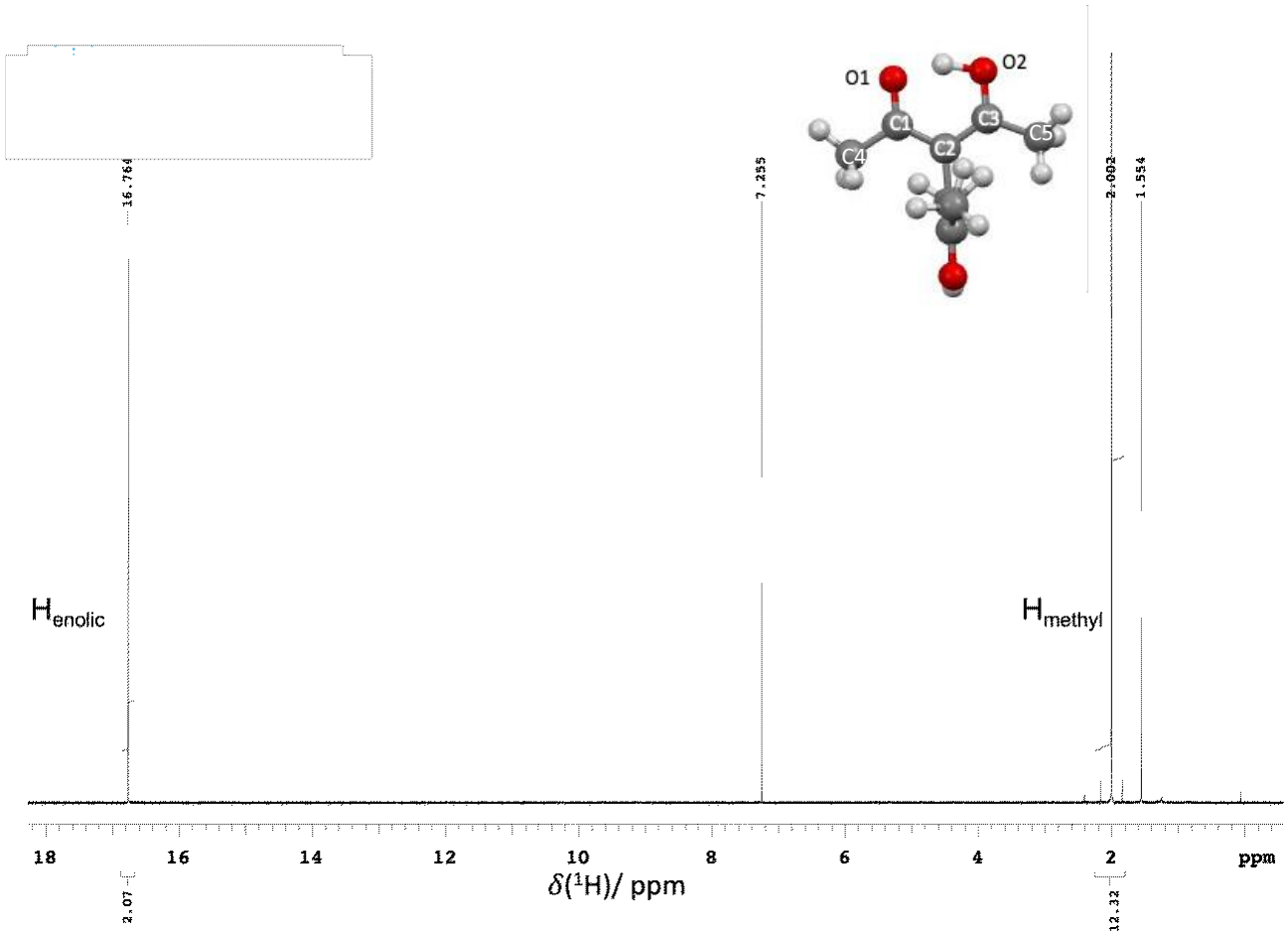

Figure 2B. ^{1}H NMR spectrum of approximately 210 mM solution of TAE in $CDCl_3$ acquired at 400 MHz and 26.9 ºC, referenced to $CDCl_3$ at 7.26 ppm. The high intensity peak at 1.56 ppm is water impurity.[9]

APPENDIX C
Tetraacetylethane: Density Functional Theory (DFT) Calculations

Experimental Methods

Cambridge Sequential Total Energy Package (CASTEP) code (versions 7.0 and 8.0).[37] CASTEP employs DFT using the plane-wave pseudopotential approach. For all calculations in this work, the generalized gradient approximation with the Perdew−Burke−Ernzerhof exchange correlation functional was chosen.[104] The NMR parameters were calculated using the gauge including the projector augmented waves (GIPAW) method implemented in the NMR module of CASTEP.[105,106]

Results Summary

The comparison of calculated and experimental chemical shifts are presented in Table 4. The chemical shifts predicted by CASTEP are based on a neutron diffraction study at 298 K and experimental C-13 shifts are from a spectrum acquired at 294 K for comparison.

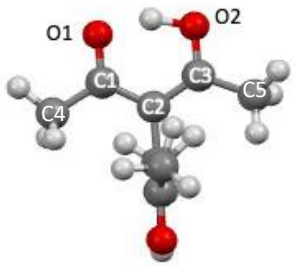

Table 1C. Comparison of CASTEP-computed and experimentally determined chemical shifts ^{13}C NMR of TAE.

C	$\sigma_{iso\ calculated}$ /ppm	$\delta_{calculated}$ /ppm	$\delta_{experimental}$ /ppm	$\delta_{experimental} - \delta_{calculated}$ /ppm
1	-30.68	210.1	198.9	-11.2
2	61.14	109.3	109.0	-0.3
3	-19.47	189.9	190.9	1.0
4	157.17	13.2	27.2	14.0
5	168.44	2.0	21.1	19.1

Parameters: $\boldsymbol{\sigma_{calc} = a\,\delta_{exp} + b}$, where $\boldsymbol{a = -1.000}$ and $\boldsymbol{b = 170.400}$

APPENDIX D
Avobenzone: Density Functional Theory (DFT) Calculations

Experimental Methods

Cambridge Sequential Total Energy Package (CASTEP) code (versions 7.0 and 8.0).[37] CASTEP employs DFT using the plane-wave pseudopotential approach. For all calculations in this work, the generalized gradient approximation with the Perdew−Burke−Ernzerhof exchange correlation functional was chosen.[104] The NMR parameters were calculated using the gauge including the projector augmented waves (GIPAW) method implemented in the NMR module of CASTEP.[105,106]

Results Summary

The comparison of calculated and experimental chemical shifts are presented in Table 1D. Overall, the chemical shifts predicted by CASTEP are close to experimental values. The most significant difference is observed in *tert*-butyl C19,19,20. Computations predict the three shifts to be distinct, while they is only one peak at 31.3 ppm experimentally.

APPENDIX D
Avobenzone: Density Functional Theory (DFT) Calculations

Table 1D. Comparison of CASTEP-computed and experimentally determined chemical shifts ^{13}C NMR of avobenzone.

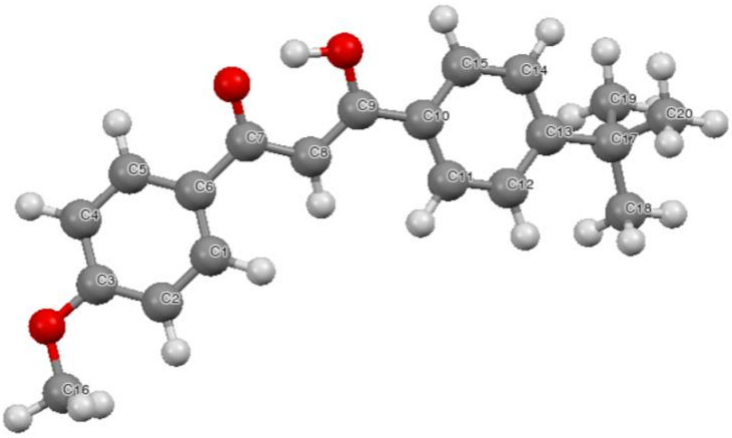

C	$\sigma_{iso\ calculated}$ /ppm	$\delta_{calculated}$ /ppm	$\delta_{experimental}$ /ppm	$\delta_{experimental} - \delta_{calculated}$ /ppm
1	36.8447	133.57	-	-
2	59.4294	110.85	111.2	0.35
3	7.3598	163.24	163.1	-0.14
4	53.6731	116.64	116.7	0.35
5	42.7322	127.65	-	-
6	40.8308	129.56	130.1	0.35
7	-20.8090	191.58	192.1	0.52
8	75.1647	95.01	93.9	0.35
9	-8.8916	179.59	181.8	2.21
10	41.5262	128.86	131.2	0.35
11	44.2745	126.09	-	-
12	44.7481	125.62	-	-
13	10.8355	159.74	157.0	-2.74
14	39.8568	130.54	-	-
15	44.2172	126.15	-	-
16	116.8567	53.07	54.6	0.35
17	134.0723	35.75	35.4	-0.35
18	143.9644	25.79	31.3	0.35
19	139.0527	30.73	31.3	0.57
20	140.5440	29.23	31.3	0.35

Parameters: $\boldsymbol{\sigma_{calc} = a\,\delta_{exp} + b}$, where $\boldsymbol{a = -1.000}$ and $\boldsymbol{b = 170.4000}$

Appendix E
Error Estimations

This section includes the error estimation for the activation energy barrier of the methoxybenzene ring flips in avobenzone.

$$k = \pi \frac{717 s^{-1}}{\sqrt{2}} = 1593\ s^{-1} \pm\ 22 s^{-1}$$

Error Estimation: $\pi \frac{\pm\ 10 s^{-1}}{\sqrt{2}} = \pm\ 22.21 s^{-1} \approx 22 s^{-1}$

$$k = \kappa\ (\frac{k_B T}{h})\ \exp\ (\frac{-\Delta \mathrm{G}\ \dagger}{RT})$$

$$1593\ s^{-1} \pm\ 22 s^{-1} = 1.0\ \mathrm{x} \frac{1.381\ \mathrm{x}\ 10^{-23}\ \mathrm{J}\ K^{-1}\ (309 \pm 2\ K)}{6.626\ \mathrm{x}\ 10^{-34}\ \mathrm{J\ s}} \exp\left(\frac{-\Delta \mathrm{G}\ \dagger}{RT}\right)$$

$$1593\ s^{-1} = 6.439\ \mathrm{x}\ 10^{12} s^{-1}\ \exp\ (\frac{-\Delta \mathrm{G}\ \dagger}{RT})$$

$$\exp\ \left(\frac{-\Delta \mathrm{G}\ \dagger}{RT}\right) = 2.474\ \mathrm{x}\ 10^{-10}$$

$$\frac{-\Delta \mathrm{G}\ \dagger}{RT} = -22.12$$

$$-\Delta \mathrm{G}\ \dagger = (-22.12)\ \mathrm{x}\ (8.314\ \mathrm{J}\ mol^{-1}\ K^{-1}\ )\ \mathrm{x}\ (309\ \mathrm{K})$$

$$\Delta \mathrm{G}\ \dagger = 56.8\ \mathrm{kJ}\ mol^{-1} \pm 1.6\ \mathrm{kJ}\ mol^{-1}$$

Error Estimation:

$$\text{Temperature Relative uncertainty} = \frac{2\ K}{309\ K}\ \mathrm{x}\ 100\% = 0.647\%$$

$$\text{Frequency Relative uncertainty} = \frac{22.21 s^{-1}}{1593\ s^{-1}}\ \mathrm{x}\ 100\% = 1.394\%$$

Appendix E
Error Estimations

$$1.394\% = 1.0 \text{ x} \frac{1.381 \text{ x } 10^{-23} \text{ J } K^{-1} \text{ x } 0.647\%}{6.626 \text{ x } 10^{-34} \text{ J s}} \exp\left(\frac{-\Delta G \dagger}{RT}\right)$$

$$1.394\% = 0.647\% \exp\left(\frac{-\Delta G \dagger}{RT}\right)$$

$$\exp\left(\frac{-\Delta G \dagger}{RT}\right) = \frac{1.394\%}{0.647\%} = 2.041\%$$

$$56.8 \text{ kJ } mol^{-1} \text{ x } 2.041\% = 1.6 \text{ kJ } mol^{-1}$$